

001
002
003
004
005
006
007
008
009
010
011
012
013
014
015
016
017
018
019
020
021
022
023
024
025
026
027
028
029
030
031
032
033
034
035
036
037
038
039
040
041
042
043
044
045
046

Microbial symbionts buffer hosts from the demographic costs of environmental stochasticity

Joshua C. Fowler^{1,2*}, Shaun Ziegler³, Kenneth D. Whitney³,
Jennifer A. Rudgers³, Tom E.X. Miller¹

¹*Department of BioSciences, Rice University, Houston, 77005, TX, USA.

²Department of Biology, University of Miami, Miami, 33146, FL, USA.

³Department of Biology, University of New Mexico, Albuquerque, 87131, NM, USA.

*Corresponding author(s). E-mail(s): jcf221@miami.edu;

Contributing authors: shaun.ziegler@gmail.com; whitneyk@unm.edu;

jrudgers@unm.edu; tom.miller@rice.edu;

Phone: 719-359-2960

Author Contributions

J.C.F. contributed to data collection, data analysis, and led manuscript drafting. S.Z. contributed to data collection and manuscript revisions. K.D.W. contributed to research conception, data collection, and manuscript revisions. J.A.R. established transplant plots, contributed to research conception, data collection, and manuscript revisions. T.E.X.M. contributed to research conception, data collection, data analysis, and manuscript revisions.

Data and Code Accessibility

Data will be made accessible as an Environmental Data Initiative package online
DOI: [updated here when available](#). Code for all analysis is available through
<https://github.com/joshuacfowler/Grass-Endophyte-Stochastic-Demography>

Article Type: Letter

Running Title: Symbiont-mediated demographic buffering

Keywords: stochasticity, demography, symbiosis, mutualism, Epichloë

This file contains: Abstract (150 words), Main Text (5397 words), Figures (1-4); Supporting Information - Supplemental Methods, Supplemental Figures A1-A28, Supplemental Tables S1-S3, References (66)

Manuscript submitted following PNAS style guidelines and can be reformatted upon revision

047

Abstract

048

Species' persistence in increasingly variable climates will depend on resilience
049 against the fitness costs of environmental stochasticity. Most organisms host
050 microbiota that shield against stressors. Here, we test the hypothesis that, by
051 limiting exposure to environmental extremes, microbial symbionts reduce hosts'
052 demographic variance. We parameterized stochastic models using data from a
053 14-year symbiont-removal experiment including seven grass species that host
054 *Epichloë* fungal endophytes. Endophytes reduced variance in fitness by > 10%, on
055 average. Hosts with "fast" life history traits that lacked longevity as an intrinsic
056 buffer benefited most from symbiont-mediated variance buffering. Under current
057 climate conditions, contributions of variance buffering were modest compared to
058 symbiont benefits to mean fitness. However, simulations of increased stochasticity
059 amplified benefits of variance buffering and made it the more important pathway
060 of host-symbiont mutualism than elevated mean fitness. Microbial-mediated
061 variance buffering is likely an important, yet cryptic, mechanism of resilience in
062 an increasingly variable world.

063

064

065

066

067

068

069

070

071

072

073

074

075

076

077

078

079

080

081

082

083

084

085

086

087

088

089

090

091

092

Introduction	093
	094
	095
	096
	097
	098
	099
	100
	101
	102
	103
	104
	105
	106
	107
	108
	109
	110
	111
	112
	113
	114
	115
	116
	117
	118
	119
	120
	121
	122
	123
	124
	125
	126
	127
	128
	129
	130
	131
	132
	133
	134
	135
	136
	137
	138

139 which symbionts may benefit their hosts instead of or in addition to elevating average
140 fitness, the focus of most previous research.

141 We used a combination of long-term field experiments and stochastic demo-
142 graphic modeling to test the hypothesis that context-dependent benefits of symbiosis
143 buffer hosts from the fitness costs of environmental stochasticity. We used cool-season
144 grasses and *Epichloë* fungal endophytes as a tractable experimental model in which
145 non-symbiotic plants can be derived from naturally symbiotic plants through heat
146 treatment, providing a contrast of symbiont effects that controls for the confounding
147 influence of host genetic background. *Epichloë* endophytes are specialized symbionts
148 growing intercellularly in the aboveground tissue of ~ 30% of *C*₃ grass species [29].
149 These fungi are primarily transmitted vertically from maternal plants through seeds
150 [30]. They produce a variety of alkaloids that can protect host plants from natural
151 enemies [31] and drought stress [32].

152 Over 14 years (2007–2021), we collected longitudinal demographic data on the
153 survival, growth, reproduction, and recruitment of all plants within replicated
154 endophyte-symbiotic and endophyte-free populations at our field site in southern Indiana,
155 USA. Through taxonomic replication (seven host-symbiont species pairs) we
156 aimed to understand whether host life history traits could explain inter-specific vari-
157 ation in the magnitude of demographic buffering through symbiosis. We used this
158 long-term data to parameterize stochastic population projection models in a hierar-
159 chical Bayesian framework. Specifically, we (1) quantified the effect of symbiosis on
160 the mean and variance of host vital rates (survival, growth and reproduction) and fit-
161 ness, (2) evaluated the relationship between host life history traits and the magnitude
162 of symbiont-mediated variance buffering, (3) determined the relative contribution of
163 symbiont-mediated mean and variance effects to host fitness, and (4) projected how
164 increased environmental stochasticity (expected under future climates) changes the
165 importance of variance buffering as a pathway of host-symbiont mutualism.
166

167 Materials and Methods

168 Study site and species

169 This study was conducted at Indiana University's Lilly-Dickey Woods Research and
170 Teaching Preserve (39.238533, -86.218150) in Brown County, Indiana, USA. This site
171 is part of the Eastern broadleaf forests of southern Indiana, where the ranges of many
172 understory cool-season grass species overlap. The experiment focused on seven of these
173 grasses (*Agrostis perennans*, *Elymus villosus*, *Elymus virginicus*, *Festuca subverticil-*
174 *lata*, *Lolium arundinaceum*, *Poa alsodes*, and *Poa sylvestris*), each of which hosts a
175 unique species of *Epichloë* endophyte (Table S1). All are native to eastern North
176 America except the Eurasian species *L. arundinaceum*.
177

178 Endophyte removal, plant propagation, and field set-up

179 Seeds from naturally symbiotic populations of the seven focal host species were col-
180 lected during summer-fall 2006 from Lilly-Dickey Woods and the nearby Bayles Road
181 Teaching and Research Preserve (39.220167, -86.542683). To generate symbiotic (S+)
182

and symbiont-free (S-) plants from the same genetic lineages, seeds from each species were disinfected with a heat treatment described in Table S1 or left untreated. The heat treatment created symbiont-free plants by warming seeds to temperatures at which the fungus becomes inviable but the host seeds can still germinate. Both heat-treated and untreated seeds were surface sterilized with bleach to remove epiphyllous microbes, cold stratified for up to 4 weeks, then germinated in a growth chamber before transfer to the greenhouse at Indiana University where they grew for ~ 8 weeks. We confirmed endophyte status by staining thin sections of inner leaf sheath with aniline blue and examining tissue for fungal hyphae at 200X magnification [33]. We established experimental populations with vegetatively propagated clones of similar sizes. By starting the experiment with plants of similar sizes and the same number of unique genotypes, we aimed to limit any potential effects of heat treatments on initial plant growth [34].

During the fall of 2007 and spring of 2008, we established 10 3x3 m. plots for *A. perennans*, *E. villosus*, *E. virginicus*, *F. subverticillata*, and *L. arundinaceum* and 18 plots for *P. alsodes* and *P. sylvestris*. Half of the plots were randomly assigned to be planted with either symbiotic (S+) or symbiont-free (S-) plants, and initiated with 20 evenly spaced individuals labeled with aluminum tags. In spring 2008, we placed plastic deer net fencing around each plot to limit deer herbivory and disturbance; damaged fences were regularly replaced.

Long-term demographic data collection

Each summer (2008–2021) we censused all individuals in each plot for survival, growth and reproduction, and added new recruits to the census. Plots contained 13.3 individuals/m² on average over the course of the experiment. Each census year was a sample of inter-annual climatic variation (n = 14 years, comprising 13 demographic transition years). We censused each species during its peak fruiting stage (May: *Poa alsodes*, *Poa sylvestris*; June: *Festuca subverticillata*; July: *Elymus villosus*, *Elymus virginicus*, *Lolium arundinaceum*; September: *Agrostis perennans*), such that the censuses were pre-breeding and new recruits came from the previous years' seed production. Leaf litter was cleared out of each plot prior to the census, to aid in locating plants. For each plant remaining from the previous year, we determined survival, measured its size as a count of tillers, and collected reproductive data as counts of reproductive tillers and seed-bearing spikelets on all reproductive tillers to a maximum of three. We also tagged all unmarked individuals that were recruits from the previous years' seed production and collected the same demographic data. New recruits typically had one tiller and were non-reproductive. In 2008 through 2010, we took additional counts of seeds per inflorescence for all reproducing individuals in the plots to relate inflorescence and spikelet counts to seed production. In 2018, we stopped collecting data for the exotic *L. arundinaceum*, which had very high survival and low recruitment, and consequently very low variation across years. In total across 14 years, the dataset included demographic information for 16,789 individual host-plants and 31,216 transition-year observations.

We expected plots to maintain their endophyte status (symbiotic or symbiont-free) because these fungal symbionts are almost exclusively vertically transmitted, and plots were spaced a minimum of 5 m apart, limiting seed dispersal or horizontal

231 transmission of the symbiont between plots. However, we regularly confirmed endo-
 232 phyte treatment throughout the lifetime of the experiment by opportunistically taking
 233 subsets of seeds from reproductive individuals and scoring them for their endophyte
 234 status with microscopy as above. Overall, these scores reflected 98% faithfulness of
 235 recruits to their expected endophyte status across species and plots (Fig. S23; Sup-
 236 plement data). Additionally, we have rarely observed fungal stromata, the fruiting
 237 bodies by which *Epichloë* are potentially transmitted horizontally, provided the fly
 238 vector is also present [35]. For *A. perennans*, *F. subverticillata*, *L. arundinaceum*, and
 239 *P. alsodes*, we never observed stromata. We observed stromata only infrequently for
 240 *E. villosus*, and even more rarely for *E. virginicus* and *P. sylvestris* (Table S2). For
 241 these species, stromata have only been observed irregularly across years on 35, 4, and
 242 6 plants respectively, making up < 0.3% of all censused plants.

243

244 Vital rate modeling

245

246 Equipped with these demographic data, we fit statistical models for survival, growth,
 247 flowering (yes or no), fertility of flowering plants (number of flowering tillers), pro-
 248 duction of seed-bearing spikelets (number per inflorescence), the average number of
 249 seeds per spikelet, and the recruitment of seedlings from the preceding year's seed
 250 production. We fit these vital rates as generalized linear mixed models in a hierar-
 251 chical Bayesian framework using RStan [36] which allowed us to isolate endophyte
 252 effects on vital rate means and variances, borrow strength across species for some
 253 variance components, and propagate uncertainty from the individual-level vital rates
 254 to population projection models [37]. All vital rate models included random plot
 255 and year effects, with separate estimates of year-to-year variance for symbiotic and
 256 symbiont-free plants, to quantify the effect of endophytes on inter-annual variance.
 257 All parameters were given vague priors [38]. We ran each vital rate model for 2500
 258 warm-up and 2500 MCMC sampling iterations with three chains. We assessed model
 259 convergence with trace plots of posterior chains and checked for \hat{R} values less than
 260 1.01, indicating low within- and between-chain variation [39, 40]. For those models
 261 that showed poor convergence, we extended the MCMC sampling to include 5000
 262 warm-up and 5000 sampling iterations, which was only necessary for seedling growth.
 263 We graphically checked vital rate model fit with posterior predictive checks comparing
 264 simulated and observed data (Fig. S19-S20).

265 *Survival* - We modeled survival as a Bernoulli process, where the survival (S) of
 266 an individual i in plot p and census year t was predicted by the plot-level endophyte
 267 status (e), host species (h), size in the preceding census, and the plant's origin status
 268 (whether it was initially transplanted or naturally recruited into the plot).

269

270

$$S_{i,p,e,h,t} \sim Bernoulli(\hat{S}_{i,p,e,h,t}) \quad (2a)$$

271

$$\text{logit}(\hat{S}_{i,p,e,h,t}) = \beta_{0_h} + \beta_1 * \text{origin}_i \quad (2b)$$

272

$$+ \beta_{2_h} * \text{endo}_e + \beta_{3_h} * \text{size}_{i,t-1} + \tau_{e,h,t} + \rho_p \quad (2c)$$

273

$$\tau_{e,h,t} \sim \text{Normal}(0, \sigma_{\tau_{e,h}}^2) \quad (2d)$$

274

275

276

$$\rho_p \sim Normal(0, \sigma_{\rho}^2) \quad (2e)$$

277

278

Here, \hat{S} is the survival probability, β_{0_h} is an intercept specific to each host species, β_1 is the effect of the plant's recruitment origin, β_{2_h} is the endophyte effect, β_{3_h} is the size effect, $\tau_{e,h,t}$ is a normally distributed year effect for each species and endophyte status with variance $\sigma_{\tau_{e,h}}^2$, and ρ_p is a normally distributed plot effect with variance σ_{ρ}^2 ($p(e)$ indicates that plot identity is uniquely associated with an endophyte status). We assume that origin effect β_1 and plot-to-plot variance σ_{ρ}^2 are shared across host species, allowing us to "borrow strength" across the multi-species dataset; other model parameters are unique to host species. We separately modeled the survival of newly recruited seedlings with a similar model but omitting previous size dependence and origin status.

Growth - We modeled plant size in census year t (G) with the same linear predictor for the mean as described for survival. Because we measured size as positive integer-valued counts of tillers, we modeled it with a zero-truncated Poisson-inverse Gaussian distribution. This distribution includes a shape parameter λ_G to account for overdispersion in the data. We additionally modeled the growth of newly recruited seedlings separately with a Poisson-inverse Gaussian model omitting size structure and the plants' origin status as with seedling survival.

Flowering - We modeled whether or not a plant was flowering during the census (P) as a Bernoulli process, with the same linear predictor for the mean as described above for survival except that size dependence for reproductive vital rates was determined by the individual's size during the same census year as opposed to its size during the previous year.

Fertility - For a plant that was flowering during the census, its fertility was the number of reproductive tillers produced (F), which we modeled as a function of size in the same census period with a zero-truncated Poisson-Inverse Gaussian distribution, with the same linear predictor for the mean as described above.

Spikelets per Inflorescence - Spikelet production (K) was recorded as integer counts on up to three inflorescences per reproducing plant. We modeled these data with a negative binomial distribution, with the same linear predictor for the mean as described above.

Seed Production per Spikelet - For individuals with recorded counts of seed production, we calculated the number of seeds per spikelet from our counts of seeds and spikelets per inflorescence, and then modeled seeds per spikelet (D) as means of a Gaussian distribution for each species and endophyte status. Because we had less detailed data across years and plants for seed production than for other reproductive vital rates, we omitted both plot and year random effects.

Seedling Recruitment - We used a binomial distribution to model the recruitment of new seedlings (R) into the plots from seeds produced in the preceding year, assuming no long-lived seed bank. We included an intercept specific to each host and endophyte status and the same random effects structure as in other models. We estimated the number of seeds per plot in the preceding year by multiplying the total number of reproductive tillers per plant by the mean number of spikelets per inflorescence and mean number of seeds per spikelet (D). For plants with missing fertility or spikelet

323 data, we used the expected number of reproductive tillers (F) or of spikelets per
 324 inflorescence from (K), drawing from the full posteriors of our models. We rounded
 325 this value to get the estimated seed production for each individual, and finally summed
 326 across all reproductive plants in each year and plot to get the total number of seeds
 327 produced.

328

329 Stochastic population model

330

331 Using the fitted vital rate models, we parameterized stochastic matrix projection mod-
 332 els including two state variables: r_t (the number of newly recruited individuals in year
 333 t), and \mathbf{n}_t (a vector including all non-seedling individuals of sizes $x \in \{1, 2, \dots, U\}$, rang-
 334 ing from one to the maximum number of tillers U). We use these two state variables to
 335 avoid having to assume demographic equivalence between seedling and non-seedling
 336 one-tiller plants. We used the same model structure for each species and endophyte
 337 status (not shown in model notation, to make it more readable).

338 The number of recruits in year $t + 1$ is given by:

339

$$340 \quad r_{t+1} = \sum_{x=1}^U P(x; \boldsymbol{\tau}_P) F(x; \boldsymbol{\tau}_F) K(x; \boldsymbol{\tau}_K) D R(\boldsymbol{\tau}_R) n_t^x \quad (3)$$

341

342 The total number of seeds produced by a maternal plant of size x is the product
 343 of the size-specific probability of flowering P , the number of reproductive tillers F ,
 344 the number of spikelets per inflorescence K , and the number of seeds per spikelet D .
 345 Multiplying by the probability of transitioning from seed to seedling R gives a per-
 346 capita rate of seedling production, which is multiplied by the number of plants of size
 347 x (n_t^x , the x^{th} element of \mathbf{n}_t) and summed over all sizes. Each function also depends
 348 on the species- and endophyte-specific year random effects for that vital rate ($\boldsymbol{\tau}$, a
 349 vector of year-specific values derived from the statistical models).

350

351 The number of y -sized plants in year $t + 1$ is given by:

352

$$353 \quad n_{t+1}^y = Z(y; \boldsymbol{\tau}_Z) B(\boldsymbol{\tau}_B) r_t + \sum_{x=1}^U S(x; \boldsymbol{\tau}_S) G(x, y; \boldsymbol{\tau}_G) n_t^x \quad (4)$$

354

355 where n_{t+1}^y is the y^{th} element of vector \mathbf{n}_{t+1} . The first term on the right hand side of
 356 Eqn. 4 represents growth (Z) and survival (B) of seedling recruits. The second term
 357 includes the survival of previously x -sized plants and the growth of survivors from size
 358 x to y , summed over all x . To avoid predictions of unrealistic growth outside of the
 359 observed size distribution, we set a ceiling on the growth function for plants at the
 360 97.5th percentile of observed sizes for each host species [41].

361

362 Each of the vital rate functions in Eqns. 3 and 4 have separate intercepts and year
 363 random effects for symbiotic and symbiont-free populations, allowing us to calculate
 364 the effect of endophyte symbiosis on the mean, variance, and coefficient of variation
 365 (CV) of λ , the dominant eigenvalue of the year- and endophyte-specific projection
 366 matrix. This model treats climate drivers implicitly through year-specific random
 367 effects. We also developed a climate-explicit version with the addition of parameters
 368 defining the relationship between either annual or growing season drought index and

each vital rate. A full description of climate-explicit methods can be found in the *Supporting Information Supplemental Methods*. 369
370
371

Life History Analysis 372

We collected metrics describing each host species' life history to test the relationship 373
between pace of life and variance buffering (Table S1). Using the Rage package [42], we 374
calculated R_0 , longevity, and generation time from our estimated transition matrices 375
using the symbiont-free mean matrix as the reference condition. We recorded seed 376
size as the average lemma length from the Flora of North America [43]. We also 377
calculated the 99th percentile of maximum observed age for each species from their 378
S- populations. Next, we fit Bayesian phylogenetic mixed-effects models using the 379
brms package [44] to test the relationship between each life history trait and the 380
effect of symbiosis on the CV of λ (a measure of variance buffering) while controlling 381
for phylogenetic non-independence between host and symbiont species. We pruned 382
species-level phylogenies of plants [45] and *Epichloë* fungi [46] to include the focal 383
species. *Agrostis perennans* was not included in the tree, and so we used the congener 384
A. hyemalis. We defined separate phylogenetic covariance matrices for each pruned 385
tree. We propagated uncertainty in the estimated variance buffering effect V with a 386
measurement error model: 387
388
389
390

$$\begin{aligned} V_{MEAN,h} &\sim Normal(V_{EST,h}, V_{SD,h}) & (5a) \\ V_{EST,h} &\sim Normal(\mu_h, \sigma) & (5b) \\ \mu &= \alpha + \beta * trait + \pi_j & (5c) \\ \alpha &\sim Normal(0, .5) & (5d) \\ \beta &\sim Normal(0, .1) & (5e) \\ \sigma &\sim Half-Normal(.04, .01) & (5f) \\ \pi_h &\sim MVN(0, \sigma_\pi \mathbf{A}) & (5g) \\ \sigma_\pi &\sim Half-Normal(0, .1) & (5h) \end{aligned}$$

Here, V_{EST} is the variance buffering effect for host species h , estimated from the 401
posterior mean (V_{MEAN}) and standard deviation (V_{SD}), propagating uncertainty 402
associated with the effect of symbiosis. The model includes an intercept (α) and a slope 403
(β) defining the relationship between the variance buffering effect and the life history 404
trait. The residual standard deviation is given by (σ). We used weakly informative 405
priors to aid model convergence. Each prior was centered at zero, except for the residual 406
standard deviation, which we centered at the standard deviation of the estimated 407
variance buffering effect, .04. The phylogenetic random effect (π), which is modeled 408
as a multivariate normal distribution, has a between-species standard deviation (σ_π) 409
structured by the phylogenetic covariance matrix \mathbf{A} . We ran each MCMC sampling 410
chain for 8000 warmup iterations and 2000 sampling iterations. We assessed model 411
convergence as described for the vital rate models. 412
413
414

415 **Mean-variance decomposition**

416 To calculate stochastic population growth rates (λ_s) for each host species and endo-
417 phyte status we simulated population dynamics for 1000 years by randomly sampling
418 from the 13 annual transition matrices, discarding the first 100 years to minimize
419 the influence of initial conditions. Sampling observed transition matrices produces
420 models that realistically capture inter-annual variation by preserving correlations
421 between vital rates [47]. We tallied the total population size at each time step as
422 $N_t = r_t + \sum_{x=1}^U n_t^x$ and calculated the stochastic growth rate as $\log(\lambda_s) = E[\log(\frac{N_t}{N_{t+1}})]$
423 [48, 49]. We calculated the total effect of endophyte symbiosis as the difference in λ_s
424 between S+ and S- populations. We propagated uncertainty from the vital rate mod-
425 els to the calculation of λ_s using 500 draws from the posterior distribution of model
426 parameters.

427 We decomposed the total endophyte effect on λ_s into contributions from effects
428 on vital rate means, variances, and their interaction. Specifically, we repeated the
429 calculation of λ_s for two additional “treatments”: (1) endophyte effects on mean vital
430 rates only, with inter-annual variances shared between S+ and S- at the S- reference
431 level for all vital rates, and (2) endophyte effects on vital rate variances only, with
432 vital rate means shared between S+ and S- at the S- reference level. The combination
433 of all four λ_s treatments (S+ vital rate means and variances, S- means and variances,
434 S+ means with S- variances, S- means with S+ variances) allowed us to quantify to
435 what extent the overall effect of symbiosis derives from changes in vital rates means,
436 variances, and their interaction. The interaction occurs because the variance penalty
437 to stochastic growth is proportional to the mean value of annual growth rates (see Eq.
438 1) such that variance is more detrimental for populations with lower average growth
439 rates.

440 To create scenarios of increased variance relative to that observed during the study
441 period, we repeated the stochastic growth rate decomposition, but sampling only a
442 subset of the 13 observed annual transition matrices. We created two scenarios of
443 increased environmental variance by sampling the transition matrices associated with
444 the six or two most extreme λ values, representing the six or two best and worst years,
445 using S- populations as the reference condition. By sampling away from an average
446 year in both directions, the six- and two- years scenarios increased the standard devi-
447 ation of yearly host growth rates by 1.3 and 2.1 times, respectively, without changing
448 mean growth rates (< 2.3% difference in $\bar{\lambda}$ between simulation treatments, Fig. S21).
449 We performed the same mean-variance decomposition for these scenarios as for the
450 ambient conditions (all 13 years sampled) for all host species described above.

451

452 **Results and Discussion**

453

454 **Symbionts buffer host demographic variance**

455 Across seven host species, eight vital rates, 14 years, and 16,789 individual plants, our
456 analysis provided the first empirical evidence of symbiont-mediated variance buffer-
457 ing. Endophytes reduced inter-annual variance for 66% (37/56) of host species-vital
458 rate combinations (average Cohen’s D for effects on vital rate standard deviation:
459

–0.15) (Fig 1A; Fig. S6 - Fig. S18). Endophytes also increased mean vital rates for the majority (36/56) of host species-vital rate combinations (average Cohen's D for effects on vital rate mean: 0.15), and benefits were particularly strong for host survival, plant growth and recruitment (Fig. 1A; Fig. S1 - Fig. S5). The magnitude of mean and variance effects differed among host species and vital rates. For example, endophytes modestly increased mean adult survival (Fig. 1C) and reduced variance in survival (Fig. 1D) for *Festuca subverticillata*, while for *Poa alsodes*, variance buffering was more apparent in seedling growth and inflorescence production (Fig 1E). Interestingly, certain vital rates showed costs of endophyte symbiosis. Symbiotic individuals of *A. perennans* grew larger than those without endophytes (Fig. 1B), yet endophytes also reduced this species' mean recruitment rates (Fig. 1A). In addition, endophyte symbiosis increased variance in seedling growth for *Elymus villosus* and *Festuca subverticillata* (Fig. 1A).

Because not all vital rates contribute equally to fitness, we used stochastic matrix models to integrate the diverse effects on vital rates described above into comprehensive measures for the mean and variance of year-to-year fitness (λ_t) and the long-run stochastic fitness that integrates both mean and variance (λ_S). On average across host species, S+ populations had greater mean fitness (> 92% confidence that endophytes increased $\bar{\lambda}$) and lower inter-annual variability in fitness (> 86% confidence that endophytes decreased the coefficient of variation of λ_t) than S- populations (Fig. 2). For some host species, the CV of λ_t declined by as much as 170% (*P. alsodes*, *F. subverticillata*), while for others, endophyte effects on variance were substantially smaller (6% lower for *E. villosus*, 16% lower for *A. perennans*), or even positive (27% increase for *E. virginicus*). When mean and variance effects of symbionts were considered together, none of the host-symbiont pairings were antagonistic (i.e., with endophytes that both decreased mean fitness and increased variance) (Fig. 2C), suggesting that variation across host species and vital rates in mean and variance effects may reflect alternative strategies that yield similar net benefits of endophyte symbiosis.

Reduced sensitivity to drought, as has been reported for some *Epichloë* symbioses [32], is a candidate mechanism that could generate a signature of variance buffering: drought conditions may have weaker fitness costs for S+ hosts, reducing fluctuations in fitness through time. Accordingly, analysis of climate-explicit matrix models indicated that, for five of seven taxa, S+ populations were less sensitive to annual or growing season drought (12-month or 3- month drought index; Standardized Precipitation-Evapotranspiration Index [50]) than S- populations (Supporting Information Text; Fig. S24-S25; Table S3). However, we did not find a strong relationship between the magnitude of variance buffering and relative drought sensitivities, suggesting that other climatic factors or other temporally-varying aspects of the environment may elicit benefits of endophyte symbiosis, including documented resistance to herbivory for six of these host taxa [51, 52].

Faster life histories predict stronger symbiont-mediated variance buffering

Theory predicts that long-lived species, those on the slow end of the slow-fast life history continuum, will be less sensitive to environmental variability than short-lived

507 species [53], a pattern which has empirical support across plants [54] and animals
508 [8, 55]. Therefore, host species with long lifespans that produce few, large offspring
509 should benefit less from symbiont-mediated variance buffering than species with fast
510 life cycles that produce many smaller offspring with low per-capita chance of success
511 [56, 57]. In support of this prediction, hosts with trait values representing faster life
512 history strategies experienced greater variance buffering from endophytes than those
513 with slow life histories (Fig. 3). Bayesian phylogenetic mixed-effects models, controlling
514 for species' relatedness, indicated that variance buffering was stronger for host species
515 with shorter lifespan (Fig. 3A; 75% probability of positive relationship with empirically
516 observed maximum plant age) and smaller seeds (Fig. 3B; 73% probability of positive
517 relationship with seed length). Other life history traits similarly had positive, but
518 weaker, support for the prediction that faster life history traits correlate with stronger
519 variance buffering (Fig. S26-S28). Considering fungal life history traits, the three host
520 species for which the net mutualism benefit was weakest (*Elymus villosus*, *Elymus*
521 *virginicus*, and *Poa sylvestris*) (Fig. 2C) were the only hosts for which we observed
522 fungal stromata, fruiting bodies capable of horizontal (contagious) transmission (Table
523 S2). This result supports the theoretical expectation that strict vertical transmission
524 drives the evolution of strong host-symbiont mutualism [20, 58]. Conclusions about
525 life histories are somewhat constrained by the narrow range of trait values among
526 closely related species in the grass sub-family Pooideae and their co-evolving symbionts.
527 Our understanding of how life history variation modulates the fitness consequences of
528 microbial symbiosis would profit from tests across a wider span of taxonomic groups
529 [59].
530

531 Contributions from variance buffering are weak relative to 532 mean effects

533 To evaluate the relative importance of mean fitness benefits and variance buffering as
534 alternative pathways of mutualism, we decomposed the overall effect of the symbiosis
535 on the stochastic growth rate λ_S using simulations from the population models in four
536 configurations. These included either the full symbiosis effect (both mean and variance
537 buffering effects), mean effects alone, variance effects alone, or neither mean nor vari-
538 ance effects. Overall, the full effect of symbiosis on λ_S , averaged across host species,
539 provided strong evidence of grass-endophyte mutualism (99% certainty of a positive
540 total effect on λ_s) (Fig. 4; see Fig. S22 for individual host species). Contributions to
541 this full effect derived from both mean and variance buffering effects, as well as a
542 slightly negative interaction (i.e., the combined influence of mean and variance effects
543 was smaller than the sum of their individual effects). Endophytes' contributions to λ_S
544 from mean effects were four times greater, averaged across species, than contributions
545 from variance buffering (Fig. 4), suggesting that, under the regime of environmen-
546 tal variability represented by our 14-year study, dampened fluctuations in fitness via
547 variance buffering was a far less important element of the benefits of symbiosis than
548 increased mean fitness. Results for individual host species were largely consistent with
549 the cross-species trends (Fig S22). The full effect of symbiosis on λ_S was positive for
550 seven out of eight host species, with statistical confidence ranging from 66% to > 99%
551 certainty. The one exception was the host species *P. sylvestris*, for which our analysis

indicated that fungal endophytes were effectively neutral in their overall fitness effect (45% and 55% posterior probability of positive and negative effects; Fig S22). 553
554
555

Variance buffering strengthens under increased environmental variability 556 557 558

Simulations of increased environmental variability, a key prediction of climate change forecasts [2], indicated that mutualism with microbial symbionts, and their variance buffering effects in particular, will take on increased importance for hosts in a more variable future climate. To simulate increased variability, we repeated the decomposition of λ_S for two alternative forecast scenarios, randomly sampling transition matrices that represented either the six most extreme years experienced by each species or the two most extreme years, subsets of the thirteen transition matrices across the 14-year study period. Increased variability elicited stronger mutualistic benefits of endophyte symbiosis (Fig. 3) than ambient variability (overall effect of the symbiosis increased by > 130%). This increase was driven by increased contributions from the variance buffering mechanism (from a 24% contribution in the ambient scenario to a 66% contribution in the most variable scenario) rather than from greater mean effects. In the most variable scenario, the relative importance of mean and variance effects reversed, with variance buffering contributions that were 1.5 times greater than contributions from mean benefits, averaged across species (Fig. 4). Thus, variance buffering – a cryptic microbial influence that manifests only over long time scales – is poised to become the dominant way in which grasses benefit from symbiosis with fungal endophytes in more variable climates of the future. 559
560
561
562
563
564
565
566
567
568
569
570
571
572
573
574
575
576
577
578
579
580
581
582
583
584
585
586
587
588
589
590
591
592
593
594
595
596
597
598

Conclusion 577 578

Ecologists increasingly recognize the importance of symbiotic microbes for host organisms and the populations, communities, and ecosystems in which their hosts reside [60–63]. Despite awareness of these ubiquitous interactions, long-term studies of microbial symbiosis are very rare. Our analysis of taxonomically-replicated, long-term field experiments that manipulated the presence/absence of fungal symbionts in plants demonstrates for the first time that heritable microbes can commonly benefit hosts not only through improved mean fitness – the focus of most previous research – but also through buffering against environmental variance. Our results provide an important advance to improve forecasts of the responses of populations (and symbionts) to increasing environmental stochasticity under global change, suggesting that, for some host species, microbial symbiosis may compensate for the lack of intrinsic tolerance of variability conferred by “slow” life history traits. We found that, relative to mean fitness benefits, symbiont-mediated variance buffering made weak contributions to host-symbiont mutualism under the current regime of environmental variability. However, variance buffering is likely to become the dominant benefit that fungal endophytes confer to grass hosts in more variable future environments. This result emerges from the context-dependent nature of grass-endophyte interactions, combined 579
580
581
582
583
584
585
586
587
588
589
590
591
592
593
594
595
596
597
598

599 with the observation that environmental stochasticity generates fluctuation in con-
600 text. These key ingredients, and thus the potential for symbiont-mediated variance
601 buffering, similarly apply to the diverse host-microbe symbioses across the tree of life.
602
603
604
605
606
607
608
609
610
611
612
613
614
615
616
617
618
619
620
621
622
623
624
625
626
627
628
629
630
631
632
633
634
635
636
637
638
639
640
641
642
643
644

Acknowledgments. We thank Mark Sheehan, Ali Campbell, Kyle Dickens, Blaise Willis, and Sar Lindner for contributions to field data collection. We also thank Volker Rudolf, Daniel Kowal, Lydia Beaudrot and Judie Bronstein for helpful comments on and discussion of this project. This research was supported by the National Science Foundation (grants 1754468 and 2208857).	645 646 647 648 649 650 651 652 653 654 655 656 657 658 659 660 661 662 663 664 665 666 667 668 669 670 671 672 673 674 675 676 677 678 679 680 681 682 683 684 685 686 687 688 689 690
Supplementary information. Supplementary information for this paper includes Supplementary Methods, Figs. A1 to A28, and Tables A1 to A3.	

691 **Figures**

692

693

694

695

696

697

698

699

700

701

702

703

704

705

706

707

708

709

710

711

712

713

714

715

716

717

718

719

720

721

Fig. 1 Endophyte symbiosis altered host vital rates.(A) Shading represents the posterior mean standardized effect size (Cohen's D) of endophyte symbiosis on mean or standard deviation of host vital rates (blue indicates that symbiosis increased the mean or standard deviation and red indicates a reduction). Endophytes' diverse vital rate effects include increased (B) mean growth of *A. perennans* and (C) mean survival probability of *F. subverticillata*. Endophyte presence also reduced inter-annual variance in (D) the survival of *F. subverticillata* and (E) the fertility of *P. alsodes*. In panels B-C, mean vital rate estimates are shown with 80% credibles along with data binned by size for symbiotic (S+) and symbiont-free (S-) plants, while in panels D-E, annual vital rate estimates are shown along with data binned by size and census year. Organism silhouettes modified from "Festuca subverticillata" by Cindy Roché and "Agrostis hyemalis" and "Poa alsodes" by Sandy Long ©Utah State University.

722

723

724

725

726

727

728

729

730

731

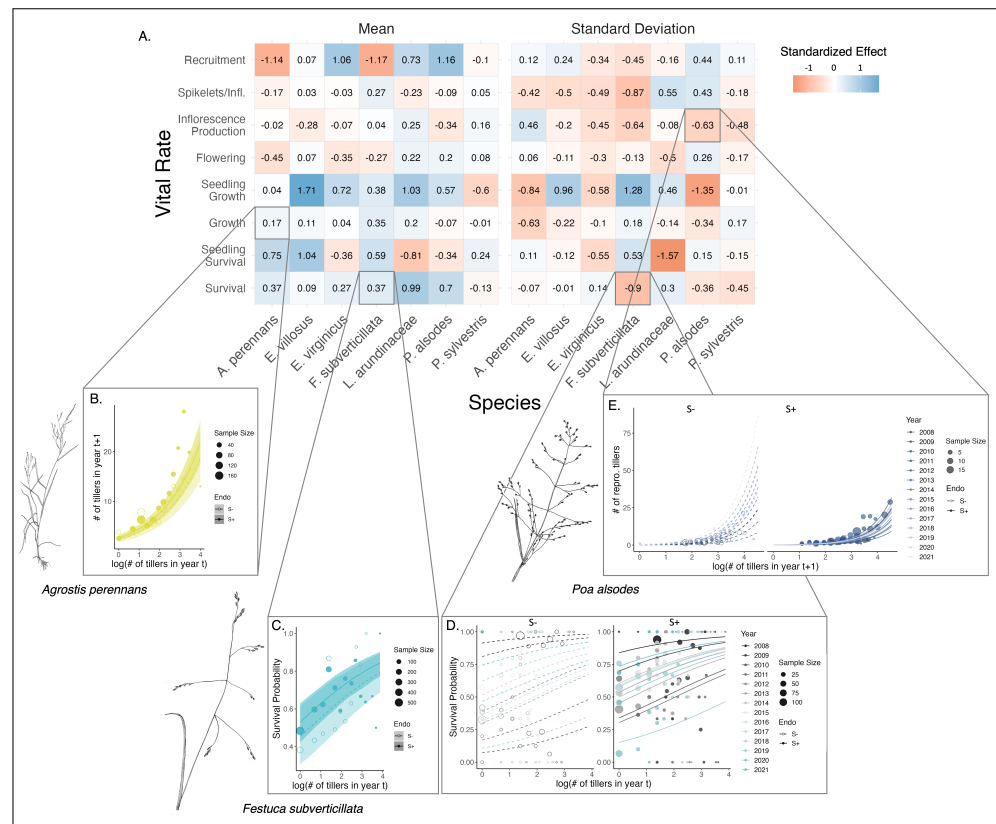
732

733

734

735

736



737
 738
 739
 740
 741
 742
 743
 744
 745
 746
 747
 748
 749
 750
 751
 752
 753
 754
 755
 756
 757
 758
 759
 760
 761
 762
 763
 764
 765
 766
 767
 768
 769
 770
 771
 772
 773
 774
 775
 776
 777
 778
 779
 780
 781
 782

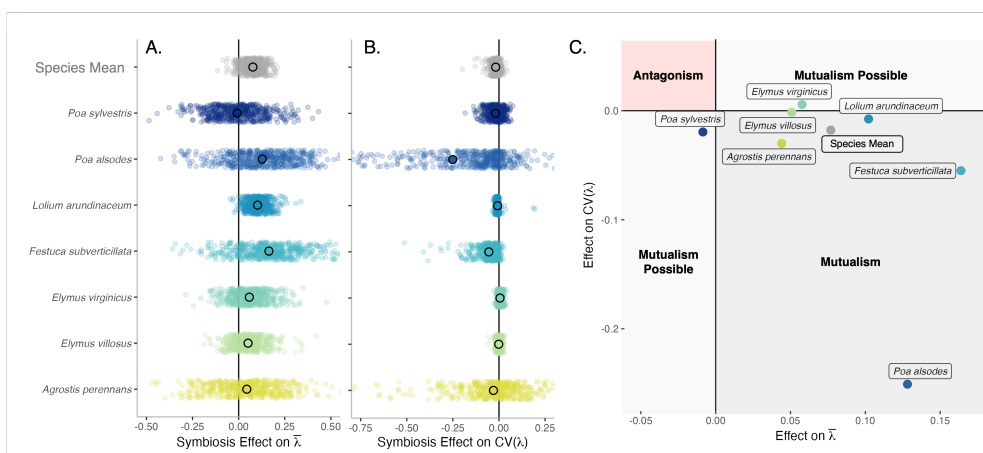


Fig. 2 Mean and variance-buffering effects on fitness. Black circles indicate the average effect of endophytes along with 500 posterior draws (smaller colored circles) on the (A) mean and (B) coefficient of variation in λ for each host species as well as a cross species mean. (C) For all hosts, endophytes either reduce variance, increase the mean, or both, and consequently when considering stochastic environments, the interactions are always at least potentially mutualistic.

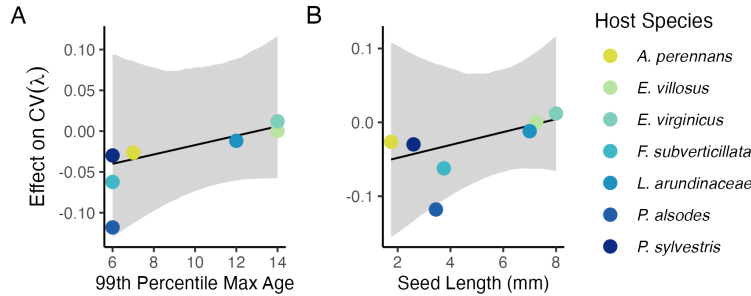
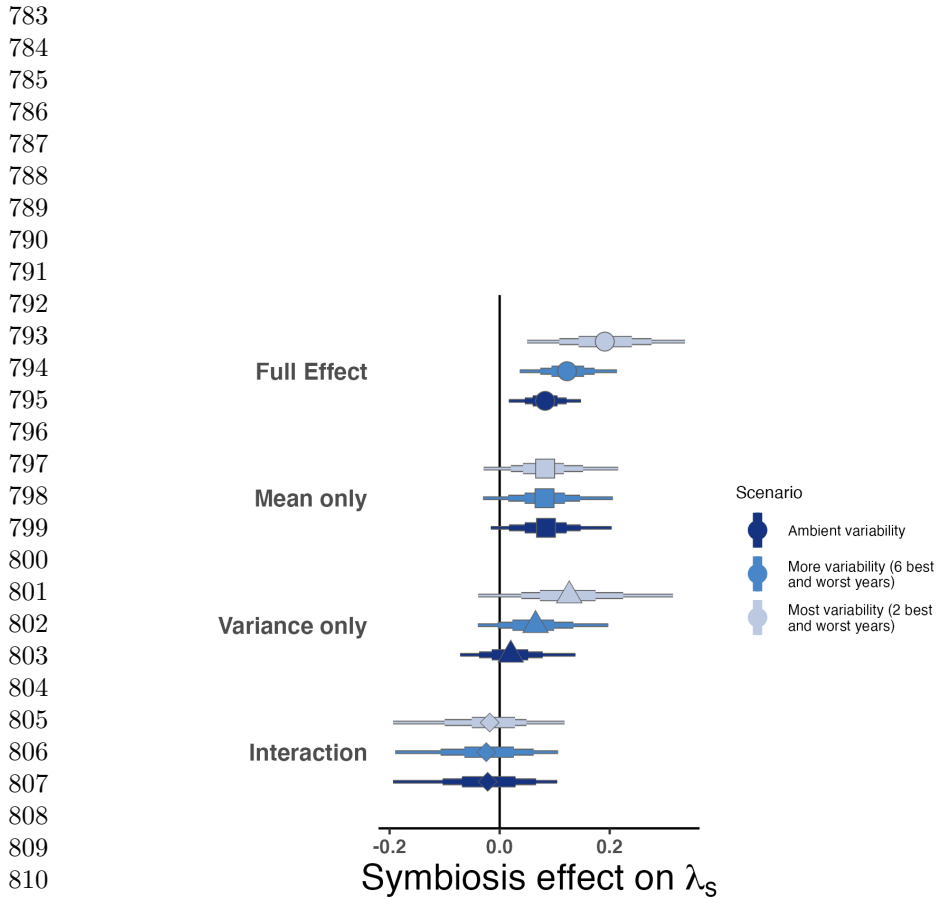


Fig. 3 Host species with faster life history traits experience stronger effects of symbiont-mediated variance buffering. Regressions between life history traits describing the fast-slow life history continuum ((A) 99th percentile maximum age observed during long term censuses in years; (B) Seed size) and the effect of endophyte symbiosis on the coefficient of variation in population growth rate (λ). Each panel shows the fitted mean relationship (line) along with the 95% credible interval.



811 **Fig. 4** Cross-species average endophyte contributions to stochastic growth rates under observed and
 812 elevated variance. Endophyte symbiosis contributes to the total effect of mutualism on λ_S through
 813 benefits to mean growth rates and through variance buffering as well as the interaction between
 814 mean and variance effects. Shapes indicate the posterior mean of each contribution averaged across
 815 the seven focal symbiota, along with bars for the 50, 75 and 95% credible intervals. The full effect of
 816 the symbiosis (circles) becomes more mutualistic under scenarios of increased variance (represented
 817 by color shading). Relative to the ambient scenario sampling transition matrices for all 13 transition
 818 years during the study period, simulations increased variance by sampling the most extreme six or
 819 two years, leading to increased contributions from variance buffering effects (triangles) and a
 820 constant contribution from mean effects (squares).

821
 822
 823
 824
 825
 826
 827
 828

Supporting Information	829
Supplemental Methods	830
Estimating climate drivers of environmental context-dependence	831
To connect the variance buffering effects of endophytes with inter-annual variability in climate, we built climate-explicit stochastic matrix population models from the vital rate data in addition to the climate-implicit model described in the main text.	832
Identifying the potentially complex relationships between vital rates and environmental drivers remains a key challenge for accurate forecasts of the ecological impacts of environmental stochasticity [64]. We first downloaded temperature and precipitation data from a weather station in Bloomington, IN, approx. 27 km from our study site, using the rnoaa package [65]. Compared to other weather stations in the area, the measurements from Bloomington contain the most complete climate record across the study period and are correlated with more local measurements from Nashville, IN for years in which local data are available (total daily precipitation: $R^2 = .76$; mean daily temperature: $R^2 = .94$). The mean annual temperature across the study period was $11.9 C^\circ$ (SD: $1.05 C^\circ$) and the average annual precipitation was 1237.9 mm/year (SD: 204.89 mm/year) (Fig. S24). Given the known role of endophytes in promoting host drought tolerance, we calculated the Standardised Precipitation-Evapotranspiration Index (SPEI) for 3 and 12 months preceding each annual censuses, reflecting drought during the growing season and across the year [50]. To calculate SPEI, we used the Thornthwaite equation to model potential evapotranspiration as implemented in the SPEI R package [66]	833
We repeated the process of fitting statistical models for each vital rate as described in Materials and Methods with the inclusion of a parameter describing the influence of SPEI. We fit separate vital rate models incorporating either the growing season or annual drought index for each vital rate, except for the model describing the mean number of seeds per inflorescence. This model was fit without climate effects because the data came from only a few years. Initial analyses indicated similar fits for models including only a linear term and those with both linear and quadratic terms describing the relationship between the climate driver and the vital rate response, and so we proceeded with models including only the linear term. We expected that including climate predictors into the models would explain some inter-annual variance in vital rates, shrinking the variance associated with the fitted year random effects. We assessed model fit with graphic posterior predictive checks and convergence diagnostics as described for the climate-implicit analysis. Finally, we next built matrix projection models incorporating the climate-dependent vital rate functions to assess the response of symbiotic (S+) vs symbiont-free (S-) populations to drought. The model is as described in Materials and Methods with the inclusion of parameters describing the slope of the relationship with SPEI. We compared the sensitivity of λ to either annual or seasonal SPEI of S+ populations ($\frac{\Delta\lambda^+}{\Delta SPEI}$) with those of S- populations ($\frac{\Delta\lambda^-}{\Delta SPEI}$) (Fig. S25; Table S).	834
Most species were slightly more responsive to growing season rather than annual drought conditions, and for most species symbiotic populations were less sensitive to	835
	836
	837
	838
	839
	840
	841
	842
	843
	844
	845
	846
	847
	848
	849
	850
	851
	852
	853
	854
	855
	856
	857
	858
	859
	860
	861
	862
	863
	864
	865
	866
	867
	868
	869
	870
	871
	872
	873
	874

875 SPEI than symbiont-free populations (Fig. S25; Table S3). However, these drought
876 indices did not explain the full extent of inter-annual variability in demographic
877 vital rates. For example, flowering in *A. perennans* had one of the strongest climate
878 signals (82% probability of a positive relationship with SPEI), yet the estimated inter-
879 annual variance $\sigma_{\tau_p}^2$ for symbiont-free plants shrank from 6.7 to 6.1 after including
880 3-month SPEI as a covariate, suggesting that other factors contribute to inter-annual
881 variability.

882

883

884

885

886

887

888

889

890

891

892

893

894

895

896

897

898

899

900

901

902

903

904

905

906

907

908

909

910

911

912

913

914

915

916

917

918

919

920

Supplemental Figures S1-S28

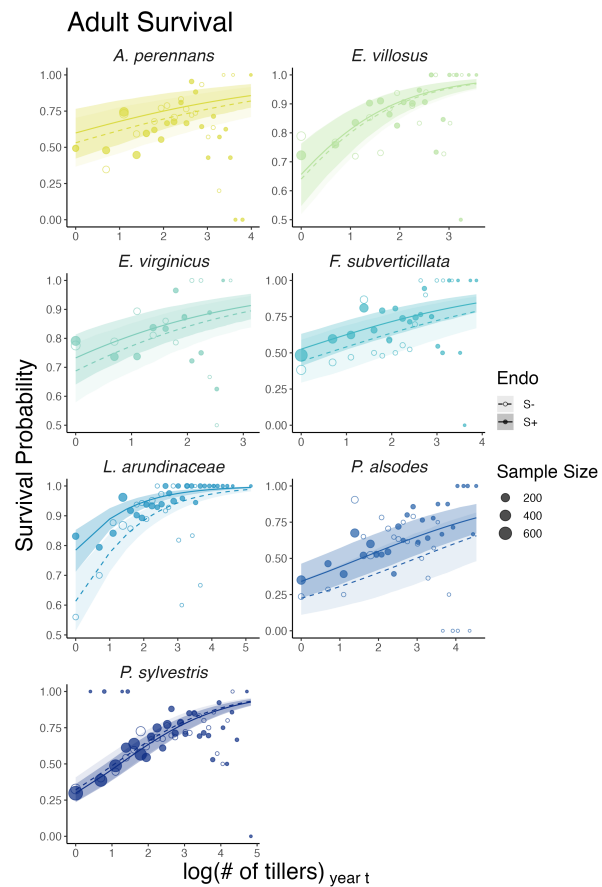
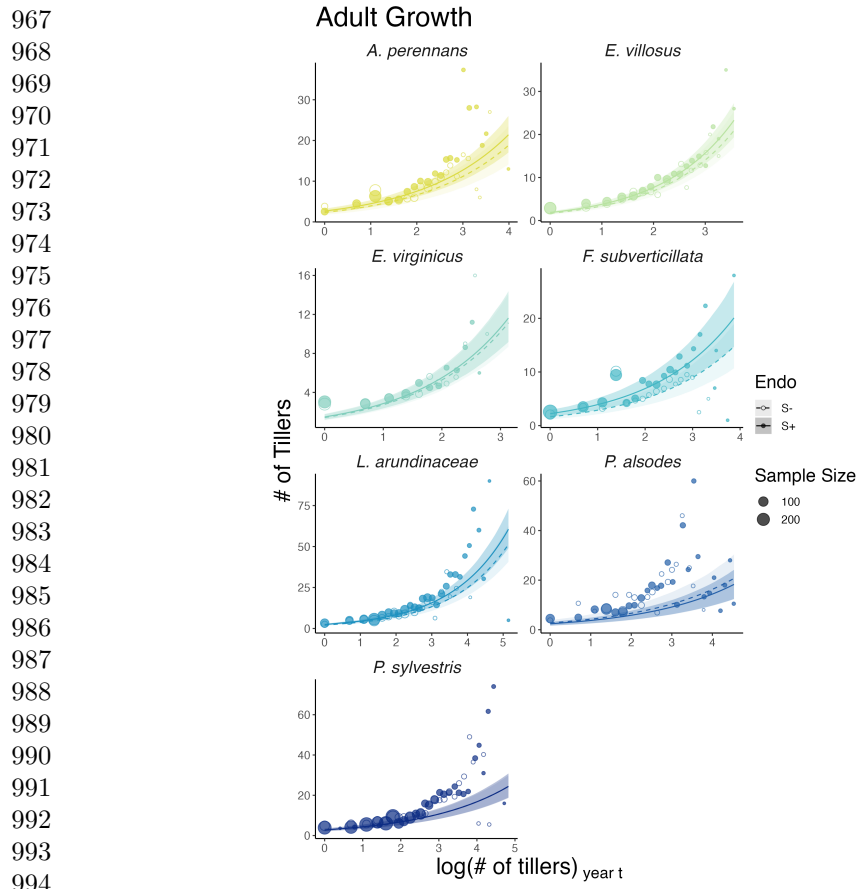


Fig. S1 Effect of endophyte symbiosis on mean adult survival. Fitted curves represent the size-specific mean survival probability along with data binned by size shown as open circles with a dashed line for symbiont-free (S-) plants, while the solid line and filled circles represent symbiotic (S+) plants. 80% credible intervals are shown with dark shading for S+, or light shading for S-.

921
922
923
924
925
926
927
928
929
930
931
932
933
934
935
936
937
938
939
940
941
942
943
944
945
946
947
948
949
950
951
952
953
954
955
956
957
958
959
960
961
962
963
964
965
966



995 **Fig. S2** Effect of endophyte symbiosis on mean adult growth. Fitted curves represent the size-specific
 996 mean expected plant size along with data binned by size shown as open circles with a dashed line
 997 for symbiont-free (S-) plants, while the solid line and filled circles represent symbiotic (S+) plants.
 998 80% credible intervals are shown with dark shading for S+, or light shading for S-.

999

1000

1001

1002

1003

1004

1005

1006

1007

1008

1009

1010

1011

1012

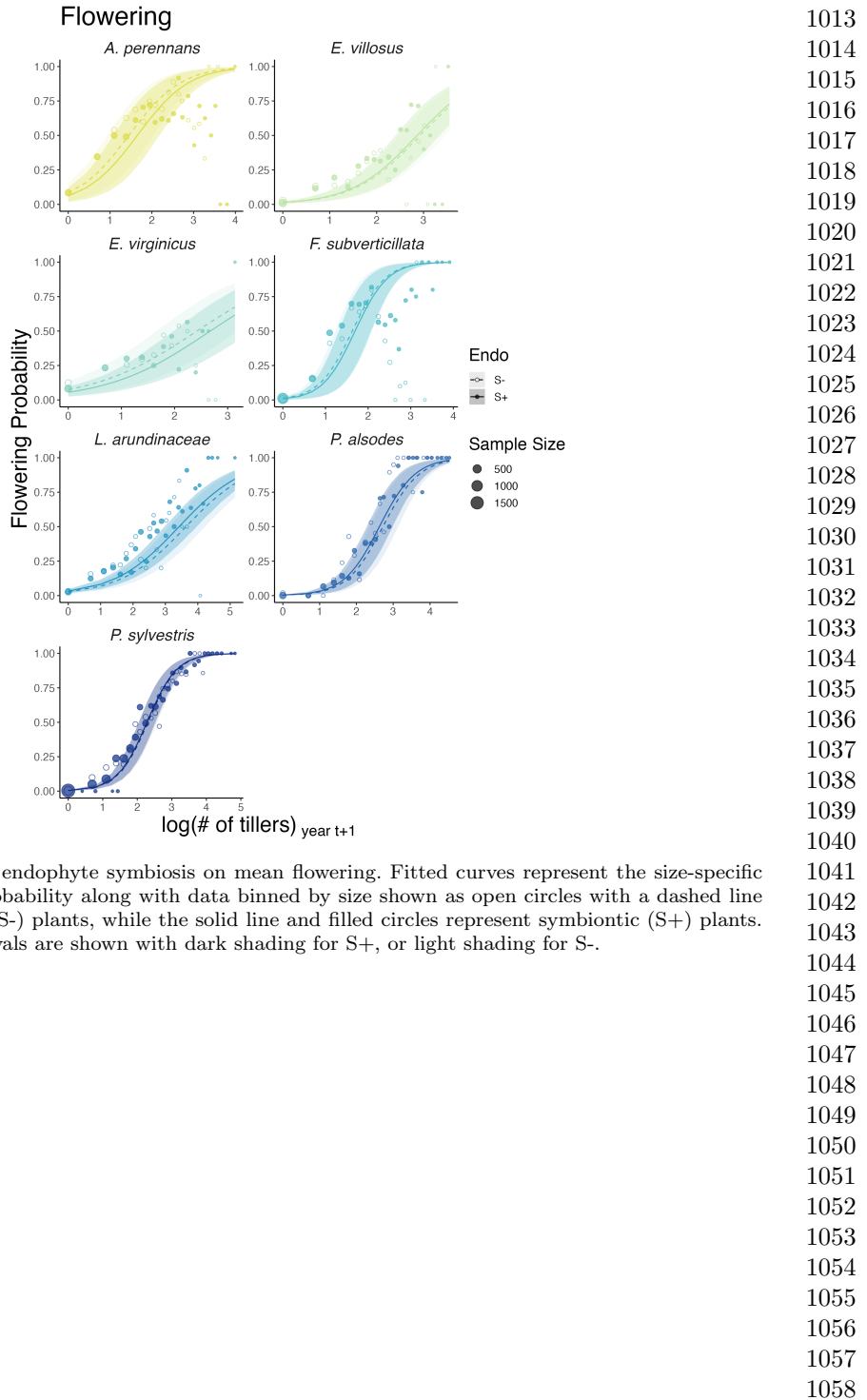
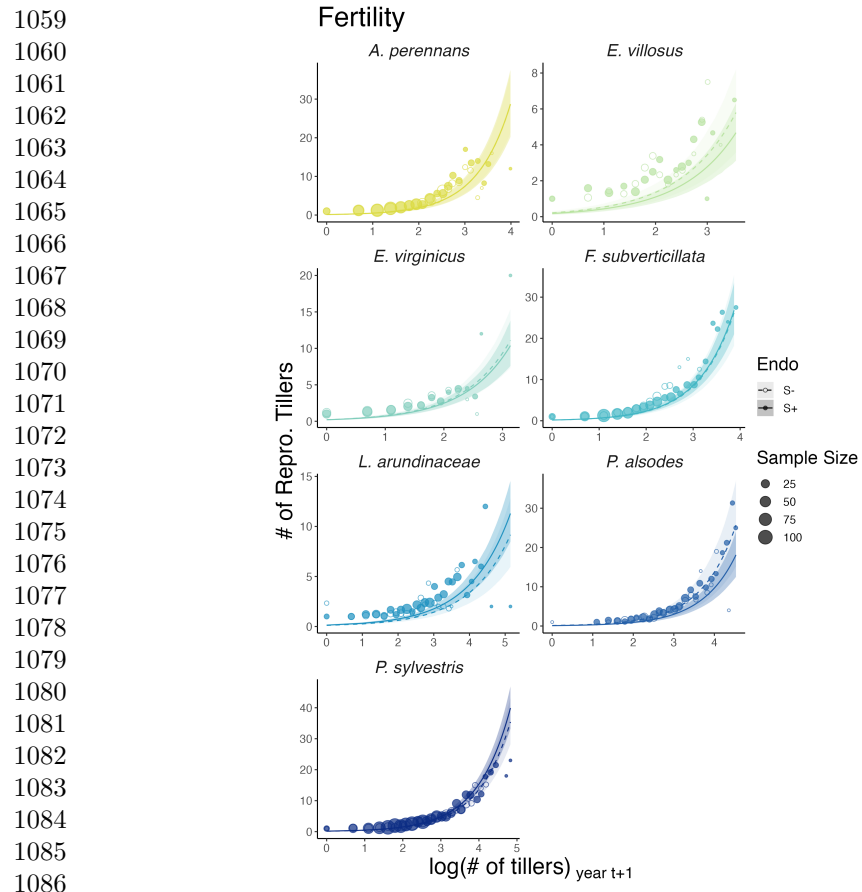


Fig. S3 Effect of endophyte symbiosis on mean flowering. Fitted curves represent the size-specific mean flowering probability along with data binned by size shown as open circles with a dashed line for symbiont-free (S-) plants, while the solid line and filled circles represent symbiotic (S+) plants. 80% credible intervals are shown with dark shading for S+, or light shading for S-.



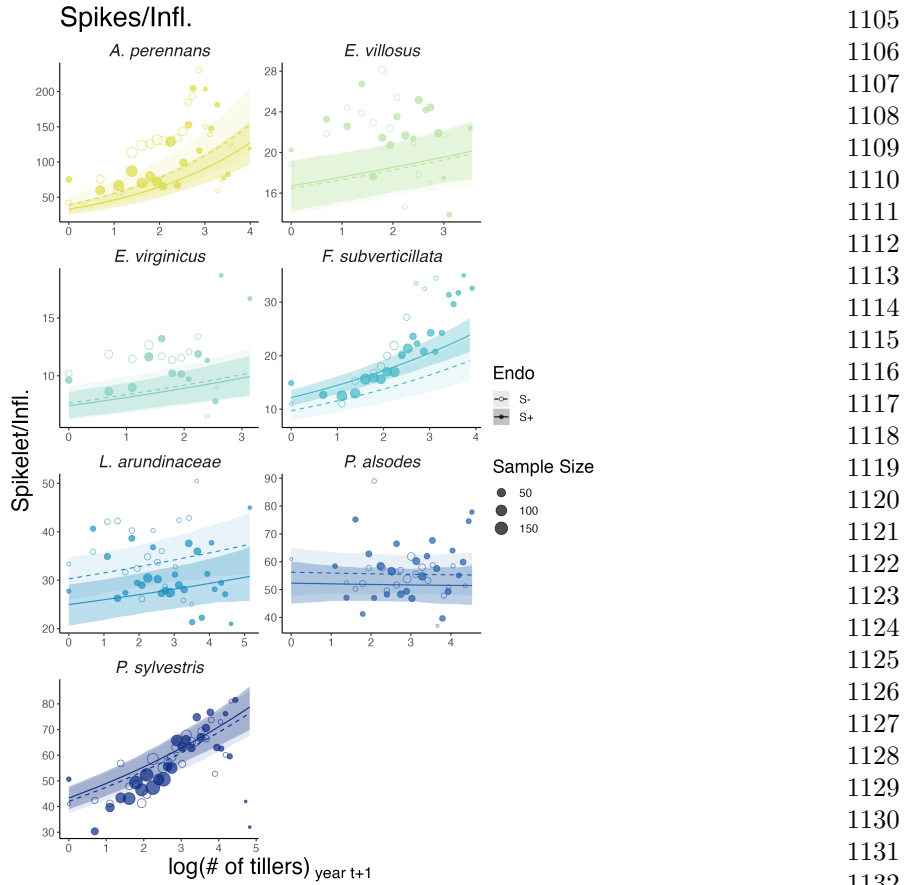
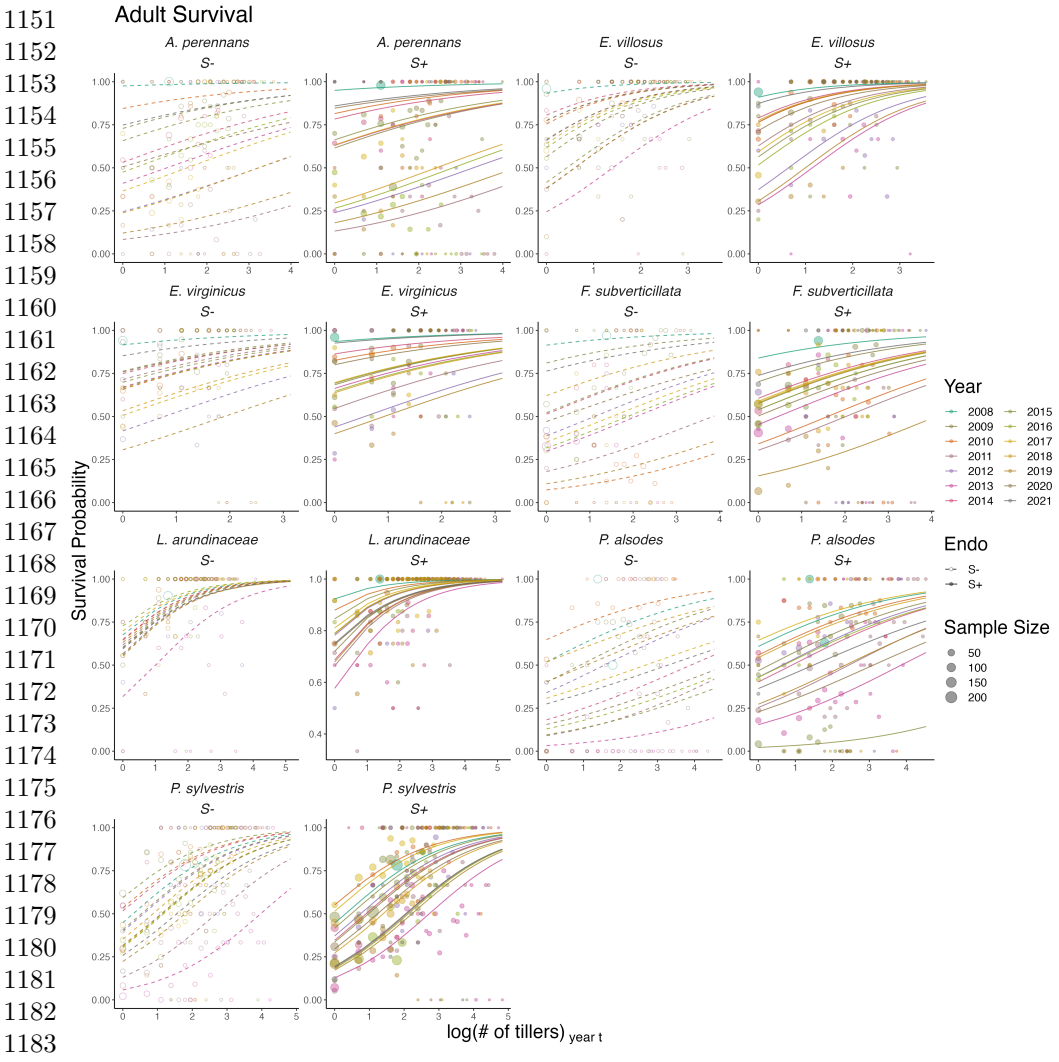


Fig. S5 Effect of endophyte symbiosis on mean spikelet production. Fitted curves represent the size-specific mean expected number of spikelets per inflorescence along with data binned by size shown as open circles with a dashed line for symbiont-free (S-) plants, while the solid line and filled circles represent symbiotic (S+) plants. 80% credible intervals are shown with dark shading for S+, or light shading for S-.

1105
1106
1107
1108
1109
1110
1111
1112
1113
1114
1115
1116
1117
1118
1119
1120
1121
1122
1123
1124
1125
1126
1127
1128
1129
1130
1131
1132
1133
1134
1135
1136
1137
1138
1139
1140
1141
1142
1143
1144
1145
1146
1147
1148
1149
1150



1183 Fig. S6 Effect of endophyte symbiosis on yearly adult survival. Fitted curves represent the size-
 1184 specific annual survival probability along with data binned by size and census year shown as open
 1185 circles with a dashed line for symbiont-free (S-) plants, while the solid line and filled circles represent
 1186 symbiotic (S+) plants.

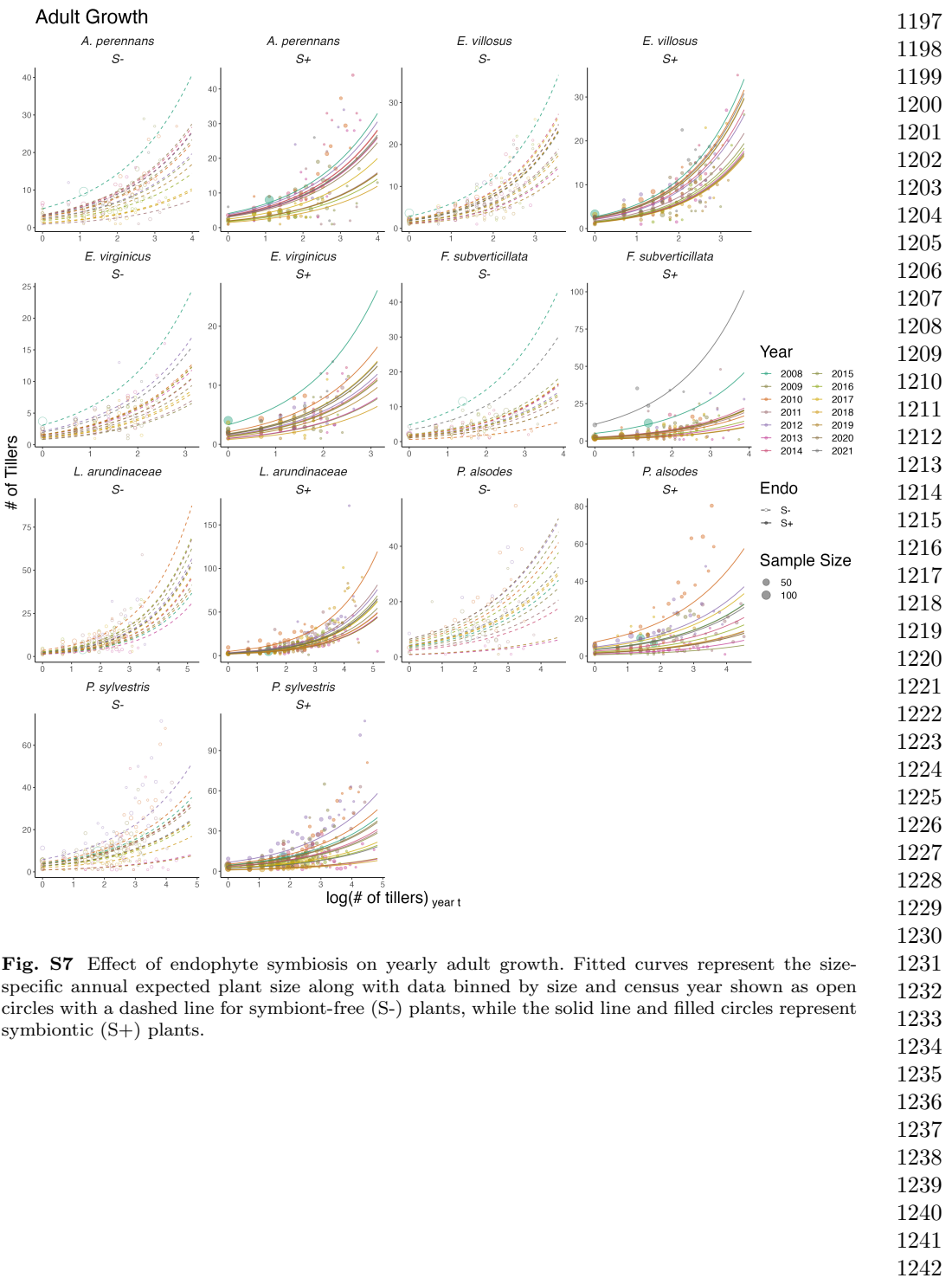
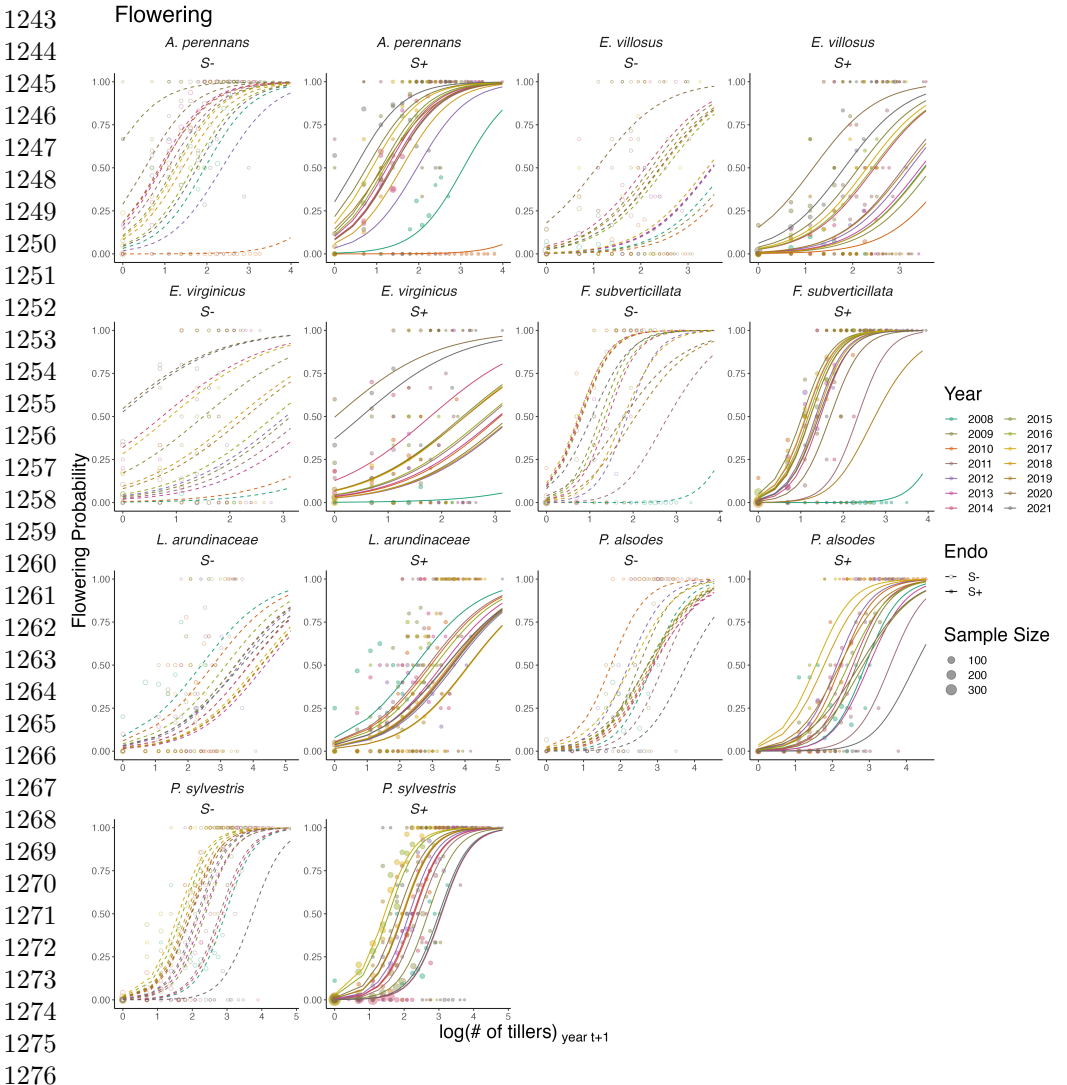


Fig. S7 Effect of endophyte symbiosis on yearly adult growth. Fitted curves represent the size-specific annual expected plant size along with data binned by size and census year shown as open circles with a dashed line for symbiont-free (S-) plants, while the solid line and filled circles represent symbiotic (S+) plants.



1277 **Fig. S8** Effect of endophyte symbiosis on yearly flowering. Fitted curves represent the size-specific
 1278 annual flowering probability along with data binned by size and census year shown as open circles with
 1279 a dashed line for symbiont-free (S-) plants, while the solid line and filled circles represent symbiotic
 1280 (S+) plants.

1281
 1282
 1283
 1284
 1285
 1286
 1287
 1288

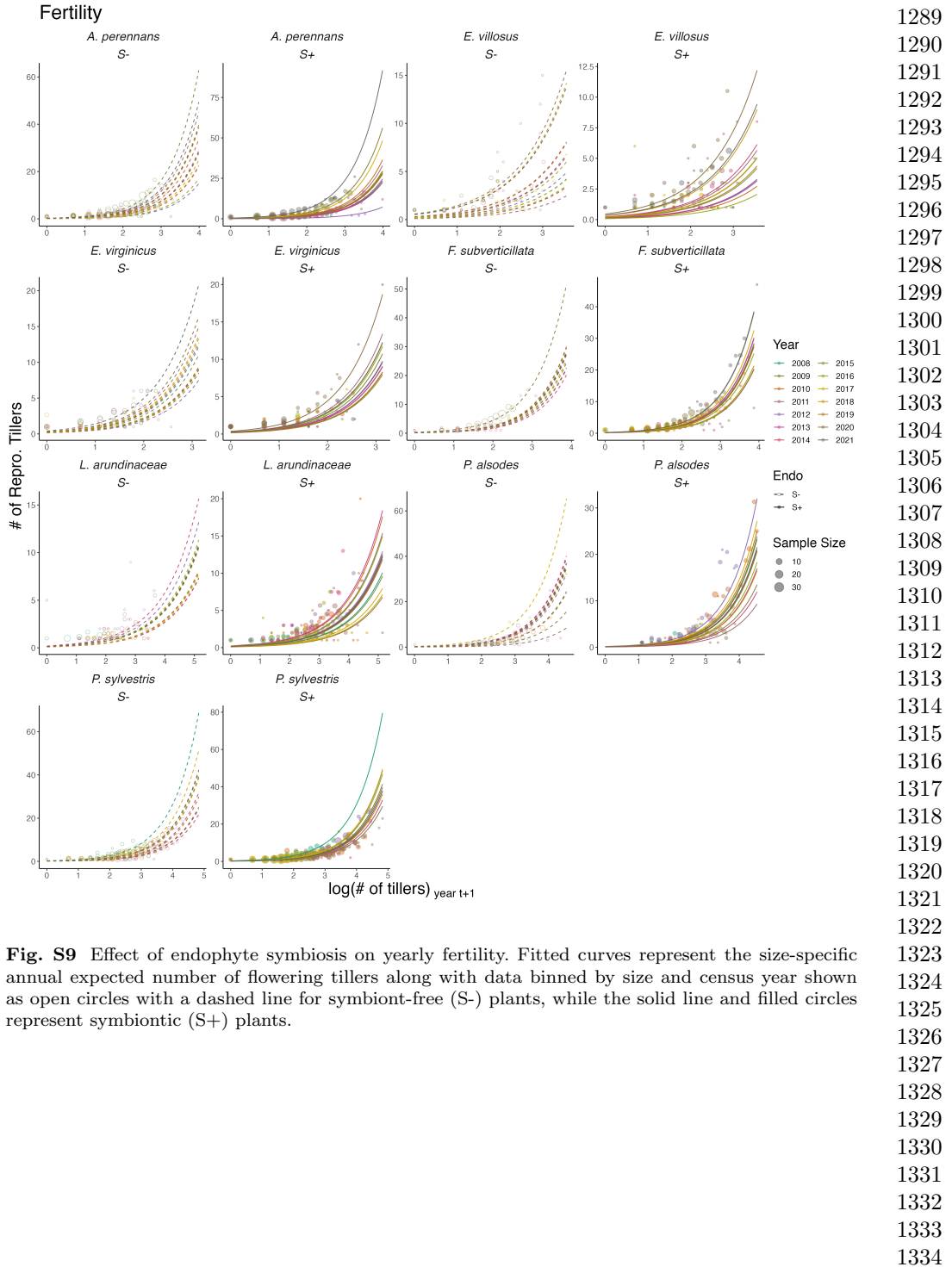
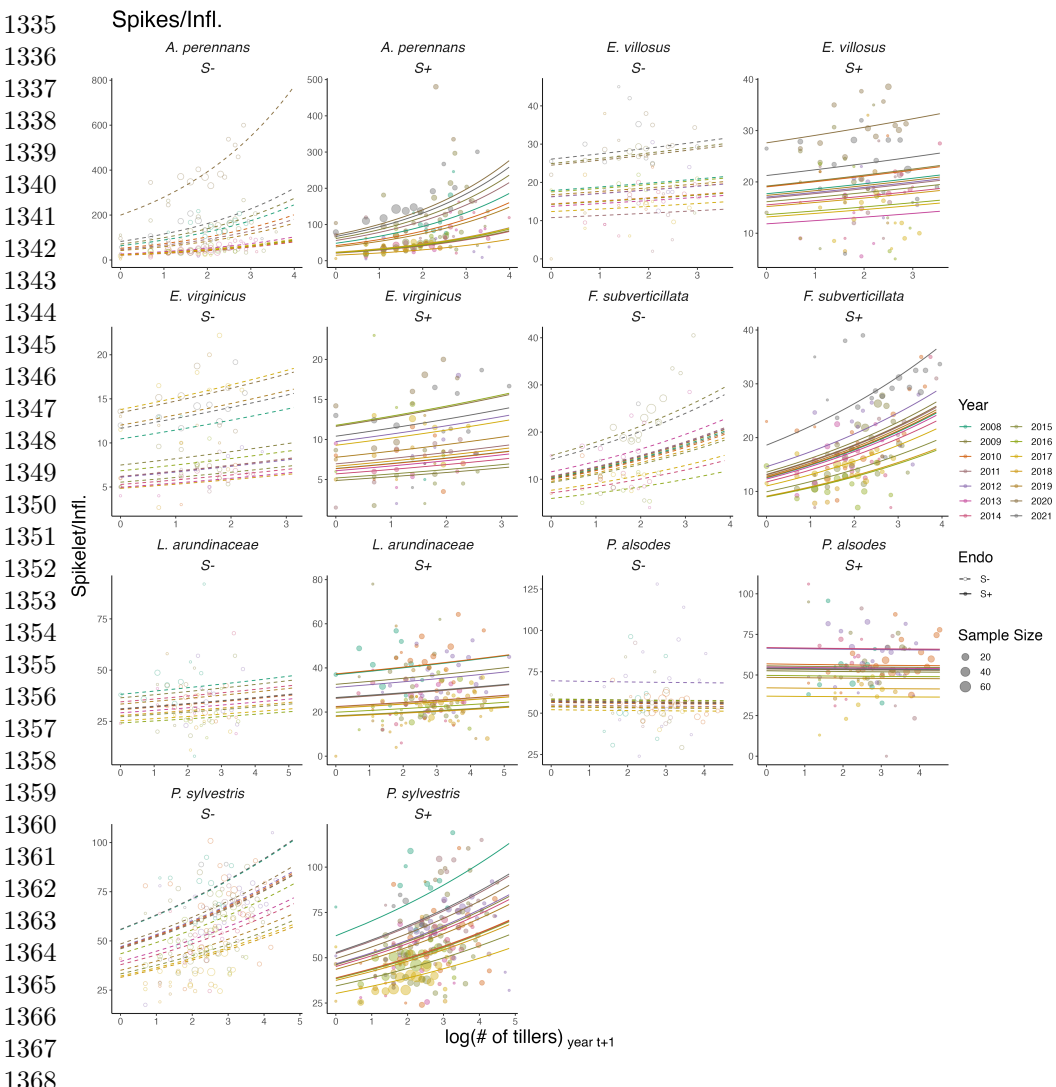


Fig. S9 Effect of endophyte symbiosis on yearly fertility. Fitted curves represent the size-specific annual expected number of flowering tillers along with data binned by size and census year shown as open circles with a dashed line for symbiont-free (S-) plants, while the solid line and filled circles represent symbiotic (S+) plants.



1369 **Fig. S10** Effect of endophyte symbiosis on yearly spikelet production. Fitted curves represent the
 1370 size-specific annual expected number of spikelets per inflorescence along with data binned by size and
 1371 census year shown as open circles with a dashed line for symbiont-free (S-) plants, while the solid line
 1372 and filled circles represent symbiotic (S+) plants.
 1373
 1374
 1375
 1376
 1377
 1378
 1379
 1380

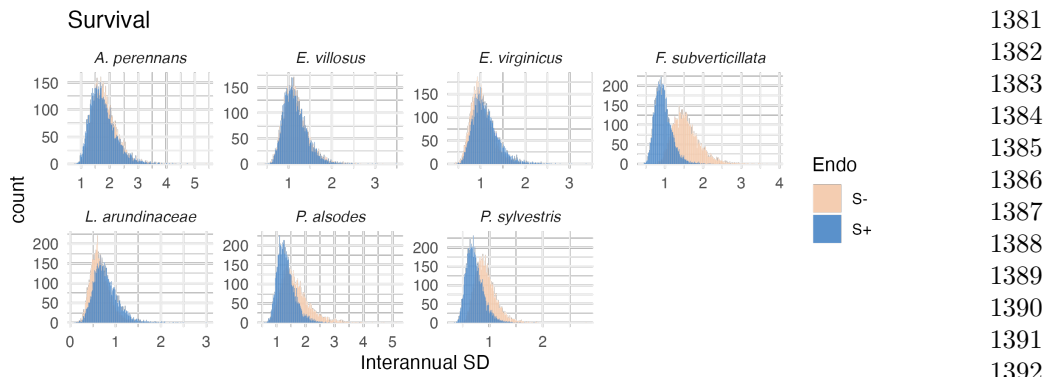


Fig. S11 Posterior distributions of the standard deviations of inter-annual year effects for survival. Histograms include 7500 post-warmup MCMC samples for symbiotic (S+; blue) and symbiont-free (S-; tan) plants from fitted vital rate model.

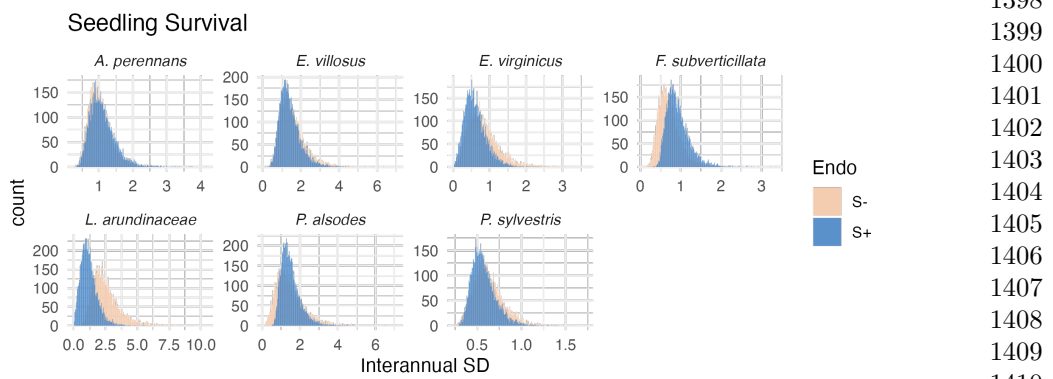
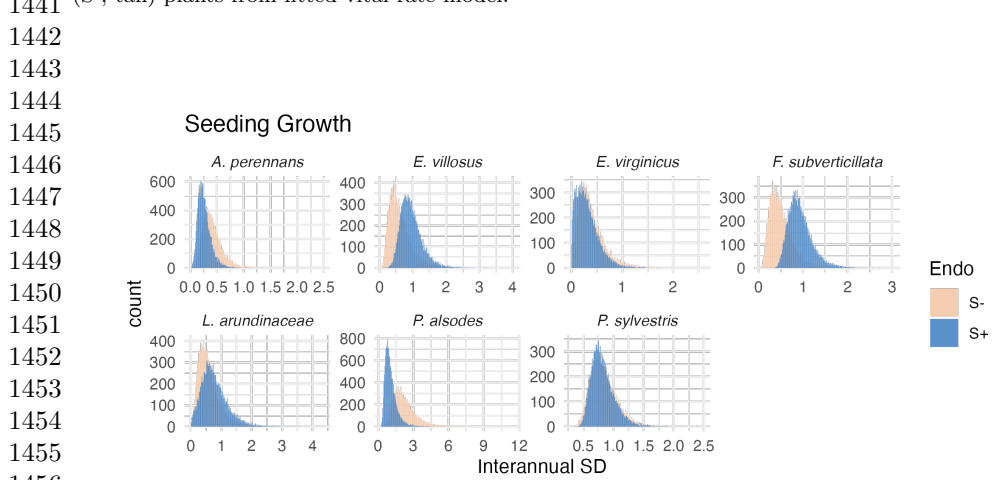
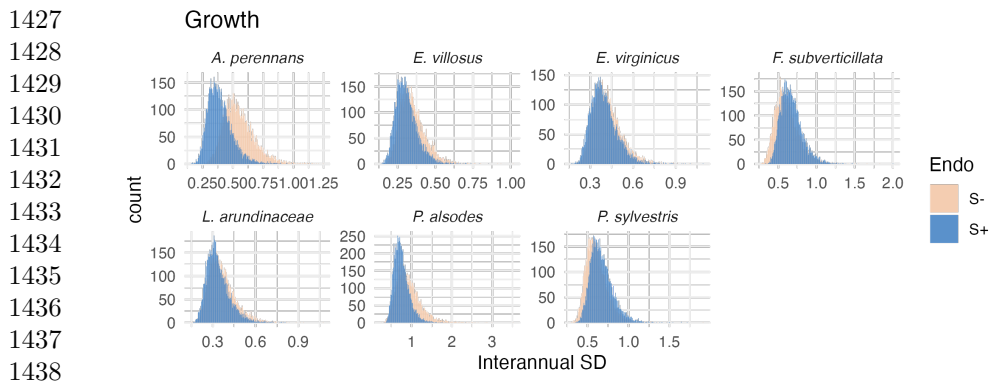


Fig. S12 Posterior distributions of the standard deviations of inter-annual year effects for seedling survival. Histograms include 7500 post-warmup MCMC samples for symbiotic (S+; blue) and symbiont-free (S-; tan) plants from fitted vital rate model.



1460

1461

1462

1463

1464

1465

1466

1467

1468

1469

1470

1471

1472

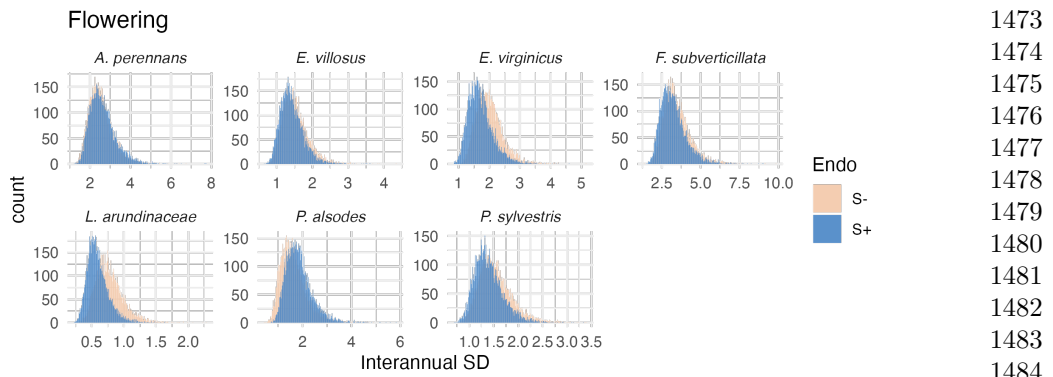


Fig. S15 Posterior distributions of the standard deviations of inter-annual year effects for flowering probability. Histograms include 7500 post-warmup MCMC samples for symbiotic (S+; blue) and symbiont-free (S-; tan) plants from fitted vital rate model.

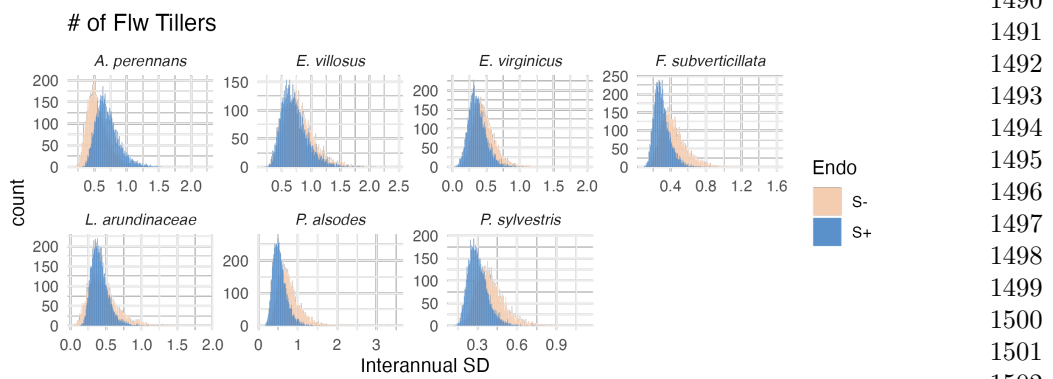
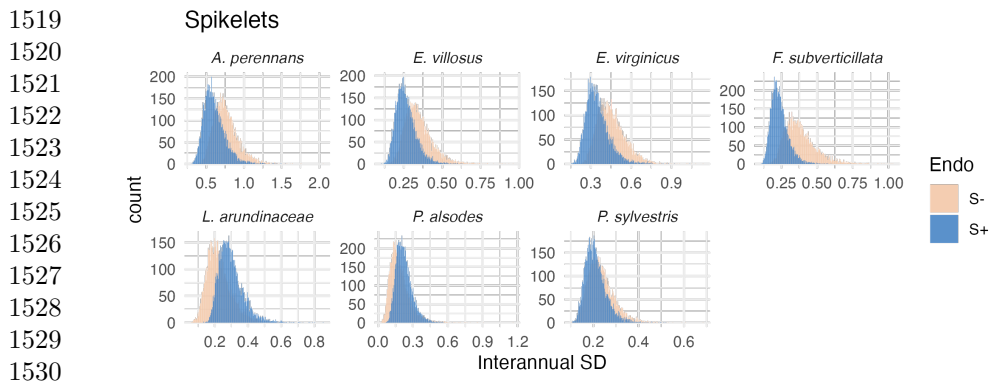
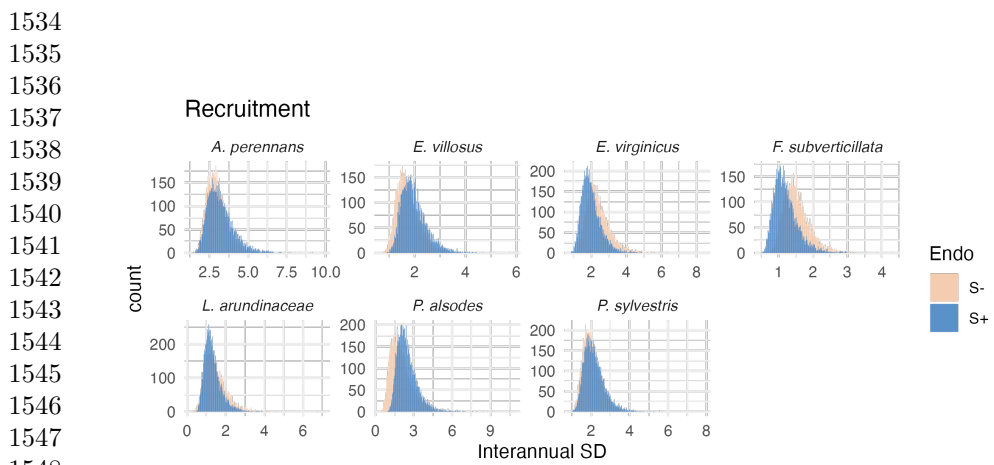


Fig. S16 Posterior distributions of the standard deviations of inter-annual year effects for fertility (no. of flowering tillers). Histograms include 7500 post-warmup MCMC samples for symbiotic (S+; blue) and symbiont-free (S-; tan) plants from fitted vital rate model.



1531 **Fig. S17** Posterior distributions of the standard deviations of inter-annual year effects for spikelets per inflorescence. Histograms include 7500 post-warmup MCMC samples for symbiotic (S+; blue) and symbiont-free (S-; tan) plants from fitted vital rate model.



1549 **Fig. S18** Posterior distributions of the standard deviations of inter-annual year effects for recruitment. Histograms include 7500 post-warmup MCMC samples for symbiotic (S+; blue) and symbiont-free (S-; tan) plants from fitted vital rate model.

1551
1552
1553
1554
1555
1556
1557
1558
1559
1560
1561
1562
1563
1564

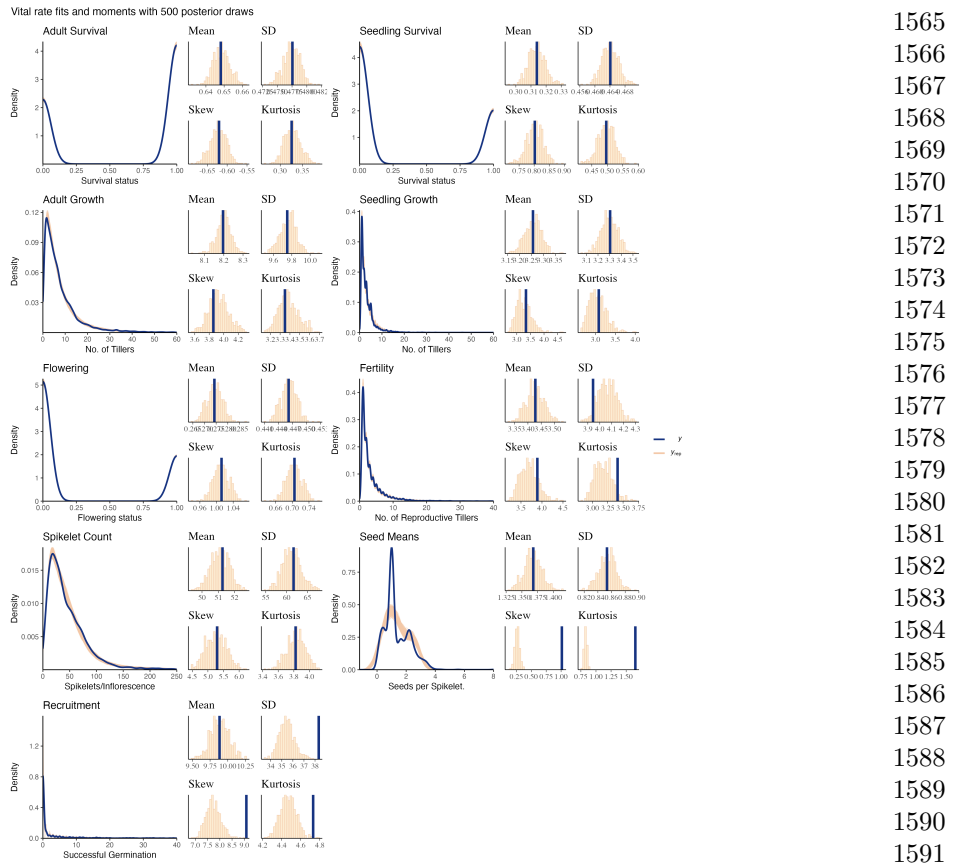
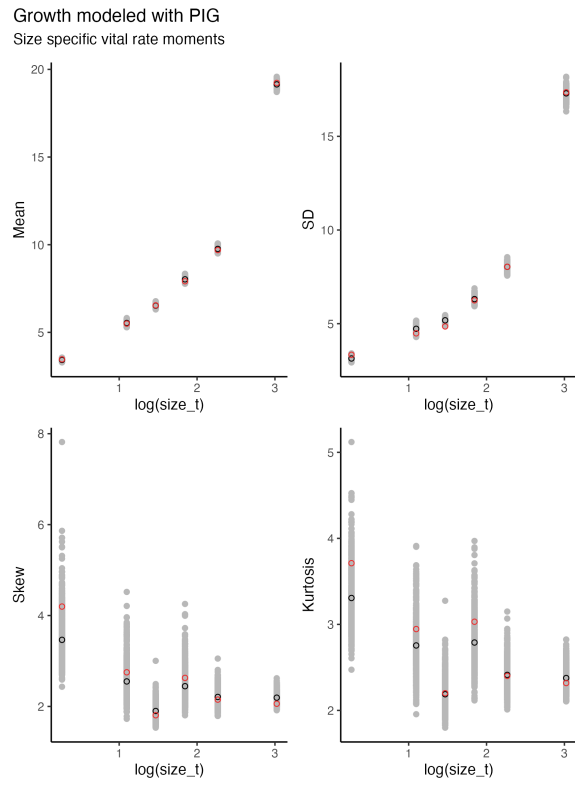


Fig. S19 Consistency between real data and simulated values indicates that fitted models describe the data well. Graphs show posterior predictive check for statistical models of demographic vital rates. Lines show density distributions of observed data (blue line) compared to data simulated from fitted models (tan lines) generated from 500 draws from posterior distributions of model parameters.

1611
1612
1613
1614
1615
1616
1617
1618
1619
1620
1621
1622
1623



1624
1625
1626
1627
1628
1629
1630
1631
1632
1633
1634
1635

1636 **Fig. S20** Consistency between real data and fitted values across sizes indicates that the growth
1637 model is accurately capturing size dependence. Graphs of posterior predictive check for mean and
1638 higher moments of the growth model across size. Points show the value of statistical moments binned
1639 across size for the observed data (red circles) compared to the simulated datasets (grey circles) and
1640 the median of the simulated values (black circles) generated from 500 posterior draws from the fitted
1641 model.

1641
1642
1643
1644
1645
1646
1647
1648
1649
1650
1651
1652
1653
1654
1655
1656

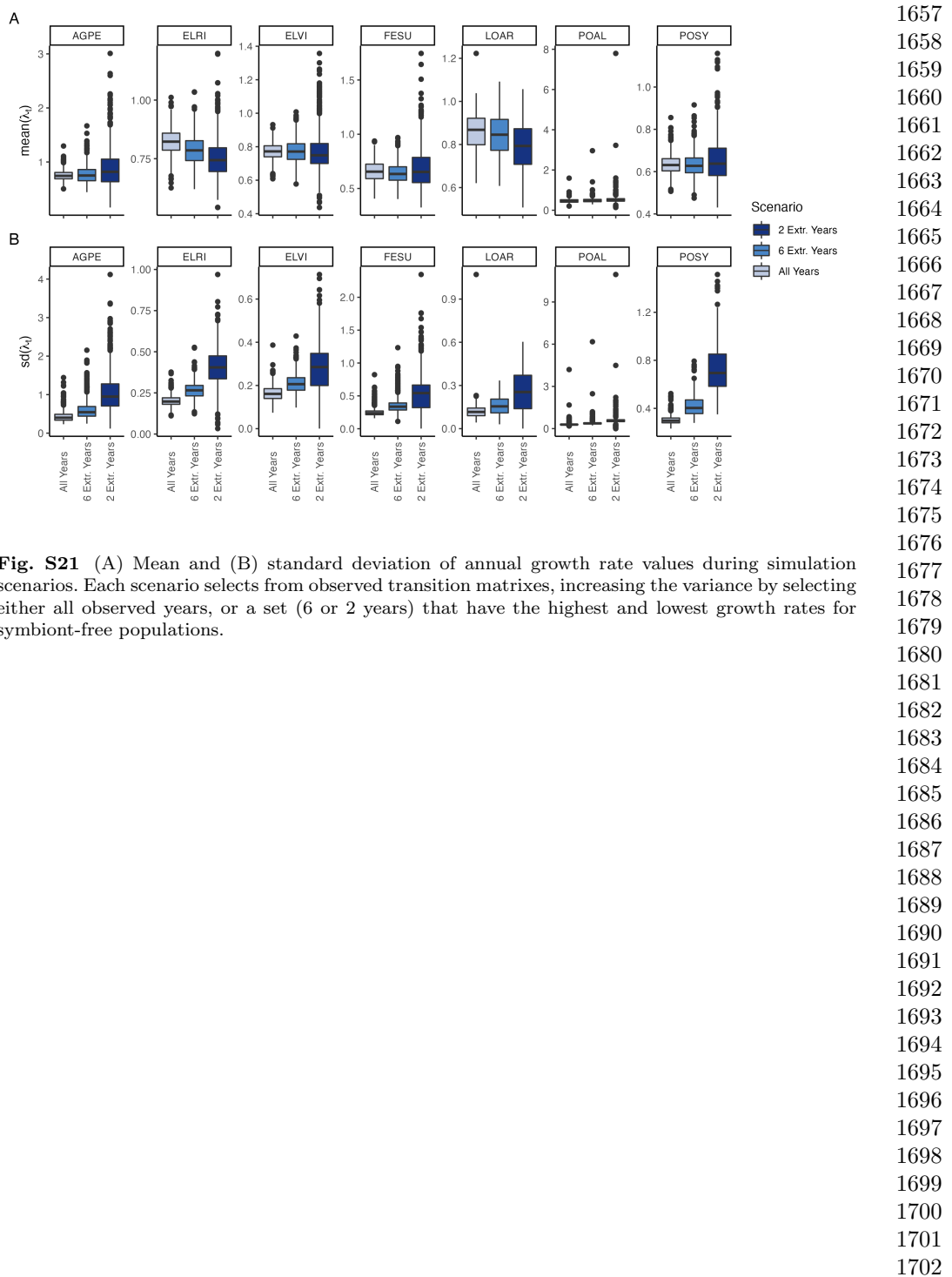


Fig. S21 (A) Mean and (B) standard deviation of annual growth rate values during simulation scenarios. Each scenario selects from observed transition matrixes, increasing the variance by selecting either all observed years, or a set (6 or 2 years) that have the highest and lowest growth rates for symbiont-free populations.

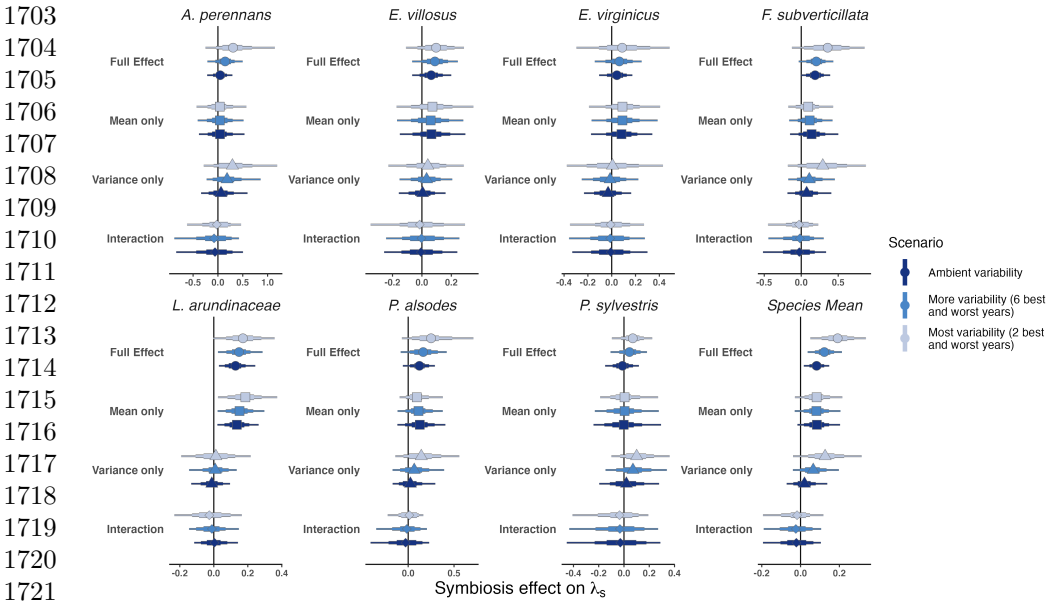


Fig. S22 Endophyte contributions to stochastic growth rates under observed and elevated variance across species. The total effect of endophytes (circle) comes from mean benefits (square) and variance buffering (triangle) as well as the interaction between mean and variance effects (diamond). Shapes indicate the posterior mean of each contribution, along with bars for the 50, 75 and 95 % credible intervals. Under scenarios of increasing variance, represented by increasing color intensity, effects of variance buffering increase leading to a more mutualistic symbiosis.

1728
1729
1730
1731
1732
1733
1734
1735
1736
1737
1738
1739
1740
1741
1742
1743
1744
1745
1746
1747
1748

Endophyte Status Checks

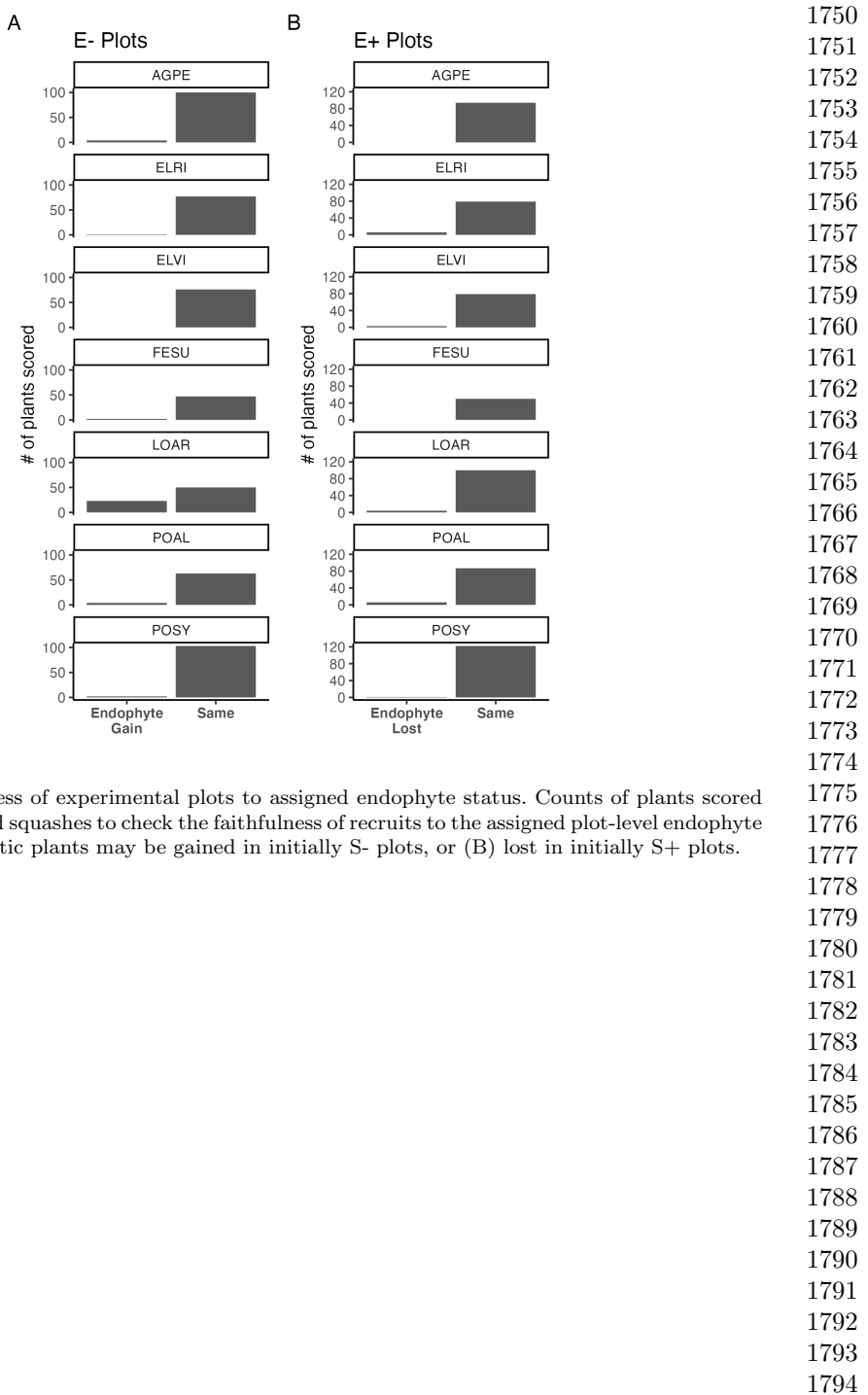


Fig. S23 Faithfulness of experimental plots to assigned endophyte status. Counts of plants scored with leaf peels or seed squashes to check the faithfulness of recruits to the assigned plot-level endophyte status. (A) Endophytic plants may be gained in initially S- plots, or (B) lost in initially S+ plots.

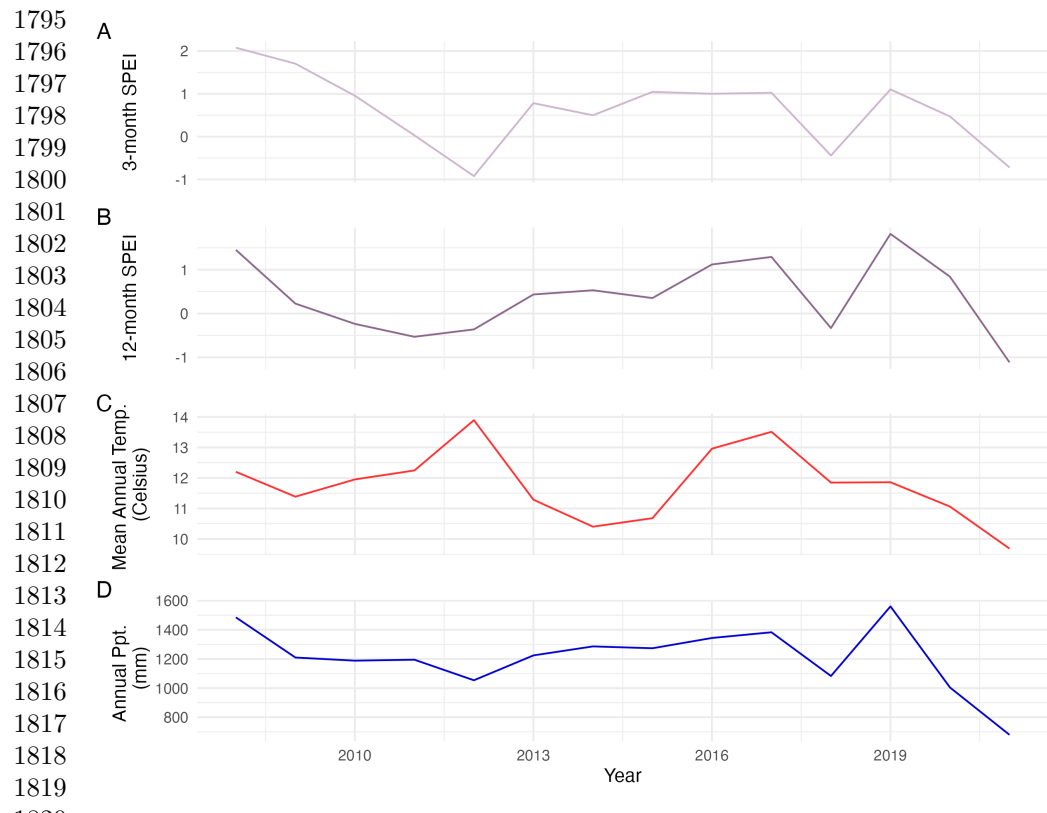


Fig. S24 Weather station time-series for Bloomington, IN. The Seasonal Precipitation-Evapotranspiration Index (SPEI) calculated for the (A) three month growing season and (B) annually from daily weather station observations of (C) average temperatures and (D) cumulative precipitation. Climatic data shown are determined by the census year centered on the month of July.

1821
1822
1823
1824
1825
1826
1827
1828
1829
1830
1831
1832
1833
1834
1835
1836
1837
1838
1839
1840

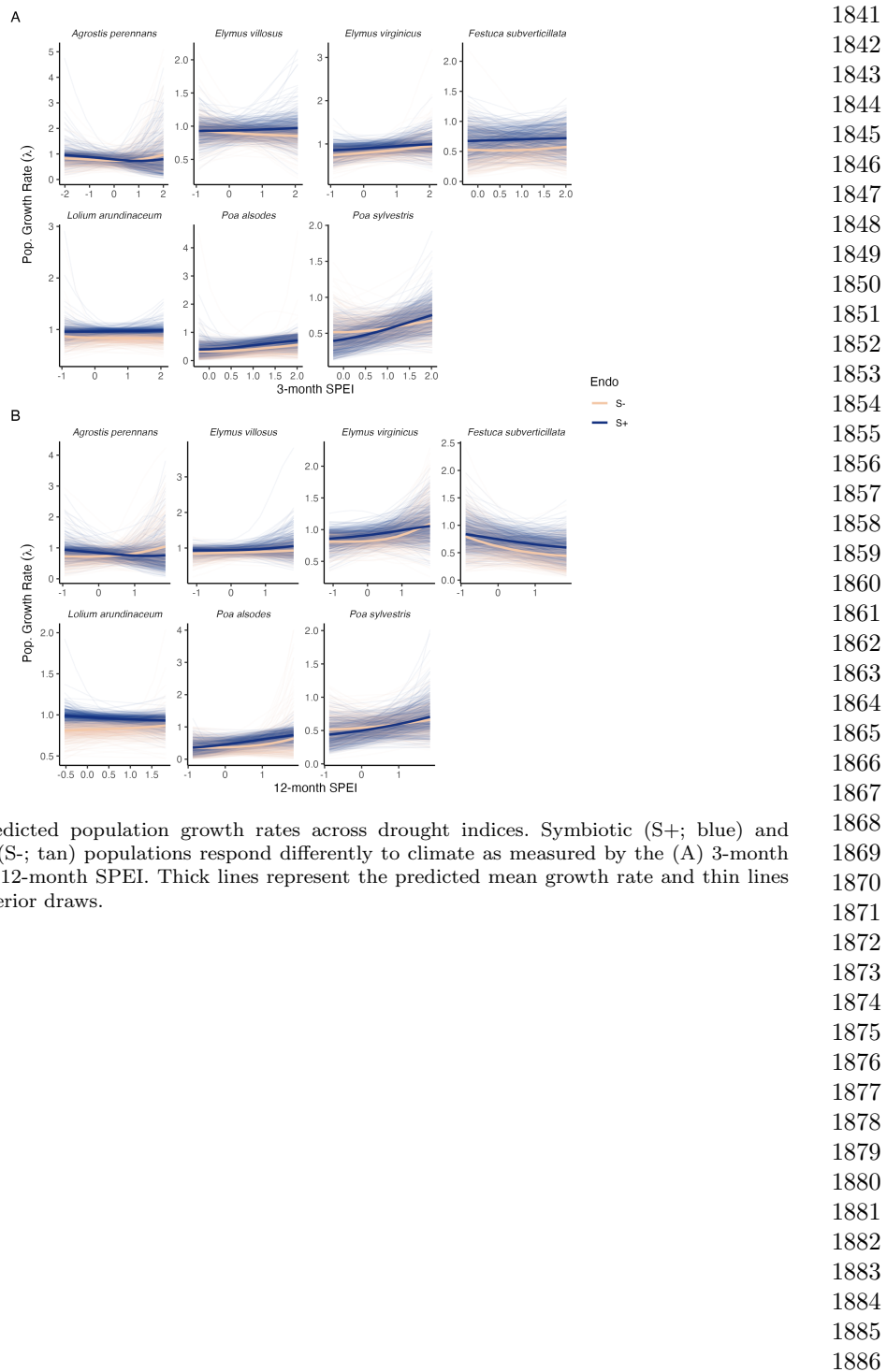


Fig. S25 Predicted population growth rates across drought indices. Symbiotic (S+; blue) and symbiont-free (S-; tan) populations respond differently to climate as measured by the (A) 3-month SPEI and (B) 12-month SPEI. Thick lines represent the predicted mean growth rate and thin lines show 500 posterior draws.

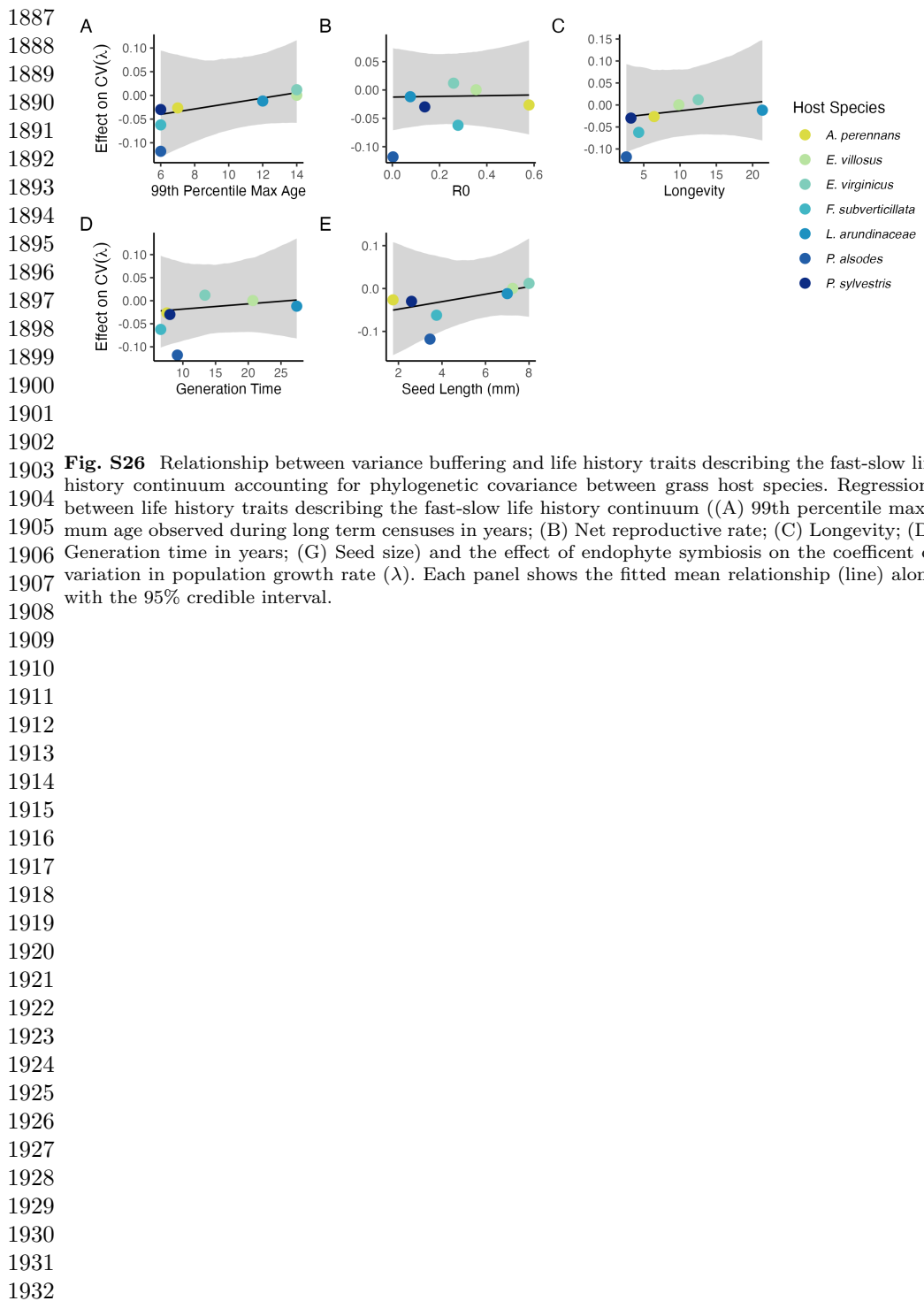


Fig. S26 Relationship between variance buffering and life history traits describing the fast-slow life history continuum accounting for phylogenetic covariance between grass host species. Regressions between life history traits describing the fast-slow life history continuum ((A) 99th percentile maximum age observed during long term censuses in years; (B) Net reproductive rate; (C) Longevity; (D) Generation time in years; (E) Seed size) and the effect of endophyte symbiosis on the coefficient of variation in population growth rate (λ). Each panel shows the fitted mean relationship (line) along with the 95% credible interval.

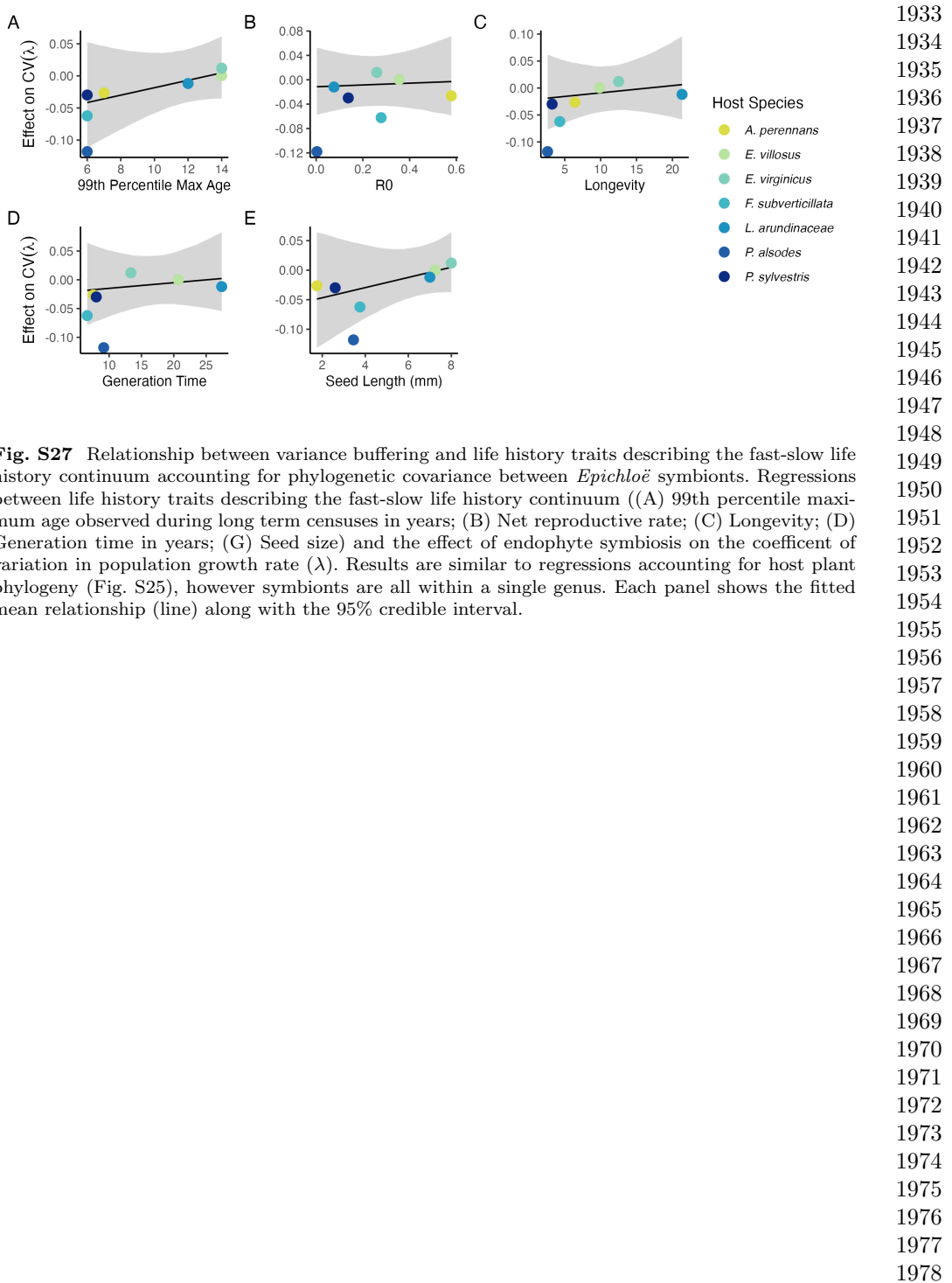


Fig. S27 Relationship between variance buffering and life history traits describing the fast-slow life history continuum accounting for phylogenetic covariance between *Epichloë* symbionts. Regressions between life history traits describing the fast-slow life history continuum ((A) 99th percentile maximum age observed during long term censuses in years; (B) Net reproductive rate; (C) Longevity; (D) Generation time in years; (E) Seed size) and the effect of endophyte symbiosis on the coefficient of variation in population growth rate (λ). Results are similar to regressions accounting for host plant phylogeny (Fig. S25), however symbionts are all within a single genus. Each panel shows the fitted mean relationship (line) along with the 95% credible interval.

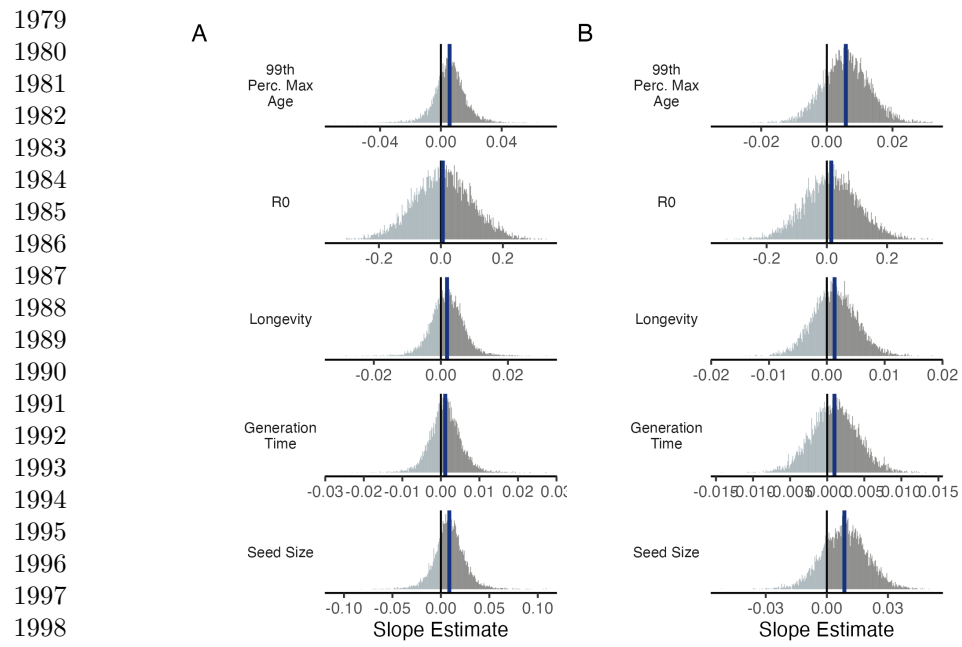


Fig. S28 Posterior estimates of life history trait effects on variance buffering. Grey histograms show the posterior distribution of the slope parameter from models incorporating (A) host plant phylogenetic covariance and (B) symbiont phylogenetic covariance for each life history trait with blue bars showing the posterior mean.

2003
2004
2005
2006
2007
2008
2009
2010
2011
2012
2013
2014
2015
2016
2017
2018
2019
2020
2021
2022
2023
2024

Supplemental Tables S1-S3

2025
2026
2027
2028
2029
2030
2031
2032
2033
2034
2035
2036
2037
2038
2039
2040
2041
2042
2043
2044
2045
2046
2047
2048
2049
2050
2051
2052
2053
2054
2055
2056
2057
2058
2059
2060
2061
2062
2063
2064
2065
2066
2067
2068
2069
2070

2071
 2072
 2073
 2074
 2075
 2076
 2077
 2078
 2079
 2080
 2081
 2082
 2083
 2084
 2085
 2086
 2087
 2088
 2089
 2090
 2091
 2092
 2093
 2094
 2095
 2096
 2097
 2098
 2099
 2100
 2101
 2102
 2103
 2104
 2105
 2106
 2107
 2108
 2109
 2110
 2111
 2112
 2113
 2114
 2115
 2116

Table S1 Summary of host-endophyte propagation and transplant methods

Host Species	Symbiont Species	Heat treatment duration (Temp.)	Transplant date
<i>Agrostis perennans</i>	<i>E. amarillans</i>	12 min. hot water bath (60 °C)	April 2008 (10 plots)
<i>Elymus villosus</i>	<i>E. elymi</i>	6 days drying oven (60 °C)	April 2008 (10 plots)
<i>Elymus virginicus</i>	<i>E. elymi</i> or <i>EviTG-1</i>	6 days drying oven (60 °C)	April 2008 (10 plots)
<i>Festuca subverticillata</i>	<i>E. starrii</i>	6 days drying oven (60 °C)	April 2008 (10 plots)
<i>Lolium arundinaceum</i>	<i>E. coenophiala</i>	6 days drying oven (60 °C)	Sept. 2007 (10 plots)
<i>Poa alsodes</i>	<i>E. alsodes</i>	7 days drying oven (60 °C)	Sept. 2007 (8 plots)/April 2008 (10 plots)
<i>Poa sylvestris</i>	<i>E. PsyTG-1</i>	7 days drying oven (60 °C)	Sept. 2007 (8 plots)/April 2008 (10 plots)

2117
2118
2119
2120
2121
2122
2123
2124
2125
2126
2127
2128
2129
2130
2131
2132
2133
2134
2135
2136
2137
2138
2139
2140
2141
2142
2143
2144
2145
2146
2147
2148
2149
2150
2151
2152
2153
2154
2155
2156
2157
2158
2159
2160
2161
2162

Table S2 Summary of focal life history traits

Host Species	Observed max age (years)	99th percentile max age (years)	Generation time (years)	R_0	Longevity (years)	Seed length (mm.)	Imperfect transmission rate (%)	Stromata Observed of indiv. per species)
<i>Agrostis perennans</i>	11	7	7.6	0.58	6.4	1.75	69.8	0.0
<i>Elymus villosus</i>	14	14	20.7	0.35	9.8	7.25	100	4.6
<i>Elymus virginicus</i>	14	14	13.4	0.25	12.5	8	100	0.6
<i>Festuca subverticillata</i>	9	6	6.6	0.28	4.3	3.75	42.7	0.0
<i>Lolium arundinaceum</i>	12*	12*	27.4	0.08	21.3	7	100	0.0
<i>Poa alsodes</i>	8	6	9.2	0.003	2.6	3.45	99.9	0.0
<i>Poa sylvestris</i>	12	6	8.0	0.14	3.2	2.6	16.6	0.1

*Censuses for *L. arundinaceum* plots stopped after year 12 of the experiment.

2163
 2164
 2165
 2166
 2167
 2168
 2169
 2170
 2171
 2172
 2173
 2174
 2175
 2176
 2177
 2178
 2179
 2180
 2181
 2182
 2183
 2184
 2185
 2186
 2187
 2188
 2189
 2190
 2191
 2192
 2193
 2194
 2195
 2196
 2197
 2198
 2199
 2200
 2201
 2202
 2203
 2204
 2205
 2206
 2207
 2208

Table S3 Summary of host-endophyte drought sensitivities

Host Species	Effect on CV(λ)	Effect on Mean(λ)	$\frac{\Delta\lambda^-}{\Delta SPEI_3}$	$\frac{\Delta\lambda^+}{\Delta SPEI_3}$	3 month S- to S+ ratio	$\frac{\Delta\lambda^-}{\Delta SPEI_{12}}$	$\frac{\Delta\lambda^+}{\Delta SPEI_{12}}$	12 month S- to S+ ratio
<i>Agrostis perennans</i>	-0.0264	0.0441	0.03	-0.04	0.85	0.11	-0.06	1.82
<i>Elymus villosus</i>	0.0003	0.0509	-0.03	0.01	1.95	0.03	0.04	0.70
<i>Elymus virginicus</i>	0.0120	0.0578	0.07	0.05	1.50	0.10	0.07	1.42
<i>Festuca subverticillata</i>	-0.0622	0.1639	0.02	0.02	1.01	-0.13	-0.09	1.43
<i>Lolium arundinaceum</i>	-0.0118	0.1022	-0.01	0.01	1.32	0.03	-0.03	1.02
<i>Poa alsodes</i>	-0.1179	0.1282	0.10	0.14	0.71	0.11	0.14	0.73
<i>Poa sylvestris</i>	-0.0298	-0.0085	0.07	0.16	0.44	0.05	0.10	0.55

References	2209
[1] Seneviratne, S. <i>et al.</i> <i>Changes in climate extremes and their impacts on the natural physical environment</i> (Cambridge University Press, 2012).	2210
[2] IPCC. Climate change 2021: The physical science basis (2021). URL https://www.ipcc.ch/report/ar6/wg1/ .	2211
[3] Lewontin, R. C. & Cohen, D. On Population Growth in a Randomly Varying Environment. <i>Proceedings of the National Academy of Sciences</i> 62 , 1056–1060 (1969). URL https://www.pnas.org/content/62/4/1056 . Publisher: National Academy of Sciences Section: Biological Sciences: Zoology.	2212
[4] Tuljapurkar, S. D. Population dynamics in variable environments. III. Evolutionary dynamics of r-selection. <i>Theoretical Population Biology</i> 21 , 141–165 (1982). URL http://www.sciencedirect.com/science/article/pii/0040580982900107 .	2213
[5] Cohen, J. E. Comparative statics and stochastic dynamics of age-structured populations. <i>Theoretical population biology</i> 16 , 159–171 (1979).	2214
[6] Tuljapurkar, S. <i>Population dynamics in variable environments</i> Vol. 85 (Springer Science & Business Media, 2013).	2215
[7] Pfister, C. A. Patterns of variance in stage-structured populations: evolutionary predictions and ecological implications. <i>Proceedings of the National Academy of Sciences</i> 95 , 213–218 (1998).	2216
[8] Morris, W. F. <i>et al.</i> Longevity can buffer plant and animal populations against changing climatic variability. <i>Ecology</i> 89 , 19–25 (2008).	2217
[9] Compagnoni, A. <i>et al.</i> The effect of demographic correlations on the stochastic population dynamics of perennial plants. <i>Ecological Monographs</i> 86 , 480–494 (2016).	2218
[10] Ellis, M. M. & Crone, E. E. The role of transient dynamics in stochastic population growth for nine perennial plants. <i>Ecology</i> 94 , 1681–1686 (2013).	2219
[11] Rodríguez-Caro, R. C. <i>et al.</i> The limits of demographic buffering in coping with environmental variation. <i>Oikos</i> 130 , 1346–1358 (2021).	2220
[12] Tuljapurkar, S. & Orzack, S. H. Population dynamics in variable environments i. long-run growth rates and extinction. <i>Theoretical Population Biology</i> 18 , 314–342 (1980).	2221
[13] Fieberg, J. & Ellner, S. P. Stochastic matrix models for conservation and management: a comparative review of methods. <i>Ecology letters</i> 4 , 244–266 (2001).	2222

- 2255 [14] Menges, E. S. Applications of population viability analyses in plant conservation.
2256 *Ecological Bulletins* 73–84 (2000).
- 2257
2258 [15] Kuparinen, A., Boit, A., Valdovinos, F. S., Lassaux, H. & Martinez, N. D.
2259 Fishing-induced life-history changes degrade and destabilize harvested ecosystems.
2260 *Scientific reports* **6**, 22245 (2016).
- 2261
2262 [16] Hilde, C. H. *et al.* The Demographic Buffering Hypothesis: Evidence and Chal-
2263 lenges. *Trends in Ecology & Evolution* **0** (2020). URL [https://www.cell.com/trends/ecology-evolution/abstract/S0169-5347\(20\)30050-1](https://www.cell.com/trends/ecology-evolution/abstract/S0169-5347(20)30050-1). Publisher: Elsevier.
- 2264
2265 [17] Rodriguez, R., White Jr, J., Arnold, A. E. & Redman, a. R. a. Fungal endophytes:
2266 diversity and functional roles. *New phytologist* **182**, 314–330 (2009).
- 2267
2268 [18] McFall-Ngai, M. *et al.* Animals in a bacterial world, a new imperative for the
2269 life sciences. *Proceedings of the National Academy of Sciences* **110**, 3229–3236
2270 (2013).
- 2271
2272 [19] Funkhouser, L. J. & Bordenstein, S. R. Mom knows best: the universality of
2273 maternal microbial transmission. *PLoS biology* **11**, e1001631 (2013).
- 2274
2275 [20] Fine, P. E. Vectors and vertical transmission: an epidemiologic perspective.
2276 *Annals of the New York Academy of Sciences* **266**, 173–194 (1975).
- 2277
2278 [21] Russell, J. A. & Moran, N. A. Costs and benefits of symbiont infection in aphids:
2279 variation among symbionts and across temperatures. *Proceedings of the Royal
2280 Society B: Biological Sciences* **273**, 603–610 (2006).
- 2281
2282 [22] Kivlin, S. N., Emery, S. M. & Rudgers, J. A. Fungal symbionts alter plant
2283 responses to global change. *American Journal of Botany* **100**, 1445–1457 (2013).
- 2284
2285 [23] Dunbar, H. E., Wilson, A. C. C., Ferguson, N. R. & Moran, N. A. Aphid thermal
2286 tolerance is governed by a point mutation in bacterial symbionts. *PLoS biology*
2287 **5**, e96 (2007).
- 2288
2289 [24] Reyna, R., Cooke, P., Grum, D., Cook, D. & Creamer, R. Detection and local-
2290 ization of the endophyte undifilum oxytropis in locoweed tissues. *Botany* **90**,
2291 1229–1236 (2012).
- 2292
2293 [25] Saikkonen, K., Gundel, P. E. & Helander, M. Chemical ecology mediated by
2294 fungal endophytes in grasses. *Journal of chemical ecology* **39**, 962–968 (2013).
- 2295
2296 [26] Neyaz, M., Gardner, D. R., Creamer, R. & Cook, D. Localization of the
2297 swainsonine-producing chaetothyriales symbiont in the seed and shoot apical
2298 meristem in its host ipomoea carnea. *Microorganisms* **10**, 545 (2022).
- 2299
2300 [27] Chamberlain, S. A., Bronstein, J. L. & Rudgers, J. A. How context dependent
 are species interactions? *Ecology letters* **17**, 881–890 (2014).

- [28] Jordano, P. Spatial and temporal variation in the avian-frugivore assemblage of prunus mahaleb: patterns and consequences. *Oikos* **479–491** (1994). 2301
2302
2303
- [29] Leuchtmann, A. Systematics, distribution, and host specificity of grass endophytes. *Natural toxins* **1**, 150–162 (1992). 2304
2305
- [30] Cheplick, G. P., Faeth, S. & Faeth, S. H. *Ecology and evolution of the grass-endophyte symbiosis* (OUP USA, 2009). 2306
2307
2308
- [31] Brem, D. & Leuchtmann, A. Epichloë grass endophytes increase herbivore resistance in the woodland grass brachypodium sylvaticum. *Oecologia* **126**, 522–530 (2001). 2309
2310
2311
2312
- [32] Decunta, F. A., Pérez, L. I., Malinowski, D. P., Molina-Montenegro, M. A. & Gundel, P. E. A systematic review on the effects of epichloë fungal endophytes on drought tolerance in cool-season grasses. *Frontiers in plant science* **12**, 644731 (2021). 2313
2314
2315
2316
2317
- [33] Bacon, C. W. & White, J. F. in *Stains, media, and procedures for analyzing endophytes* 47–56 (CRC Press, 2018). 2318
2319
2320
- [34] Rudgers, J. A. & Swafford, A. L. Benefits of a fungal endophyte in elymus virginicus decline under drought stress. *Basic and Applied Ecology* **10**, 43–51 (2009). 2321
2322
2323
2324
- [35] Bultman, T. L., White Jr, J. F., Bowdish, T. I., Welch, A. M. & Johnston, J. Mutualistic transfer of epichloë spermatia by phorbis flies. *Mycologia* **87**, 182–189 (1995). 2325
2326
2327
- [36] Stan Development Team. RStan: the R interface to Stan (2022). URL <https://mc-stan.org/>. R package version 2.21.7. 2328
2329
2330
- [37] Elderd, B. D. & Miller, T. E. Quantifying demographic uncertainty: Bayesian methods for integral projection models. *Ecological Monographs* **86**, 125–144 (2016). 2331
2332
2333
2334
- [38] Gabry, J., Simpson, D., Vehtari, A., Betancourt, M. & Gelman, A. Visualization in bayesian workflow. *Journal of the Royal Statistical Society Series A: Statistics in Society* **182**, 389–402 (2019). 2335
2336
2337
2338
- [39] Brooks, S. P. & Gelman, A. General methods for monitoring convergence of iterative simulations. *Journal of computational and graphical statistics* **7**, 434–455 (1998). 2339
2340
2341
2342
- [40] Gelman, A. & Hill, J. *Data analysis using regression and multilevel/hierarchical models* (Cambridge university press, 2006). 2343
2344
2345
2346

- 2347 [41] Williams, J. L., Miller, T. E. & Ellner, S. P. Avoiding unintentional eviction from
2348 integral projection models. *Ecology* **93**, 2008–2014 (2012).
- 2349
- 2350 [42] Jones, O. R. *et al.* Rcompadre and rage—two r packages to facilitate the use of
2351 the compadre and comadre databases and calculation of life-history traits from
2352 matrix population models. *Methods in Ecology and Evolution* **13**, 770–781 (2022).
- 2353
- 2354 [43] Flora of North America Editorial Committee Poaceae. *Flora of North America*
2355 *North of Mexico [Online]* **24**, <http://floranorthamerica.org/Poaceae> (1993+). .
- 2356
- 2357 [44] Bürkner, P.-C. brms: An R package for Bayesian multilevel models using Stan.
2358 *Journal of Statistical Software* **80**, 1–28 (2017).
- 2359
- 2360 [45] Zanne, A. E. *et al.* Three keys to the radiation of angiosperms into freezing
2361 environments. *Nature* **506**, 89–92 (2014).
- 2362
- 2363 [46] Leuchtmann, A., Bacon, C. W., Schardl, C. L., White Jr, J. F. & Tadicch,
2364 M. Nomenclatural realignment of neotyphodium species with genus epichloë.
Mycologia **106**, 202–215 (2014).
- 2365
- 2366 [47] Metcalf, C. J. E. *et al.* Statistical modelling of annual variation for inference
2367 on stochastic population dynamics using integral projection models. *Methods in*
2368 *Ecology and Evolution* **6**, 1007–1017 (2015).
- 2369
- 2370 [48] Caswell, H. Matrix population models: Construction, analysis, and interpretation.
2371 2nd edn sinauer associates. Inc., Sunderland, MA (2001).
- 2372
- 2373 [49] Rees, M. & Ellner, S. P. Integral projection models for populations in temporally
2374 varying environments. *Ecological Monographs* **79**, 575–594 (2009).
- 2375
- 2376 [50] Vicente-Serrano, S. M., Beguería, S. & López-Moreno, J. I. A multiscalar drought
2377 index sensitive to global warming: the standardized precipitation evapotranspi-
2378 ration index. *Journal of climate* **23**, 1696–1718 (2010).
- 2379
- 2380 [51] Rudgers, J. A. & Clay, K. An invasive plant–fungal mutualism reduces arthropod
2381 diversity. *Ecology Letters* **11**, 831–840 (2008).
- 2382
- 2383 [52] Crawford, K. M., Land, J. M. & Rudgers, J. A. Fungal endophytes of native
2384 grasses decrease insect herbivore preference and performance. *Oecologia* **164**,
2385 431–444 (2010).
- 2386
- 2387 [53] Murphy, G. I. Pattern in life history and the environment. *The American*
2388 *Naturalist* **102**, 391–403 (1968).
- 2389
- 2390 [54] Compagnoni, A. *et al.* Herbaceous perennial plants with short generation time
2391 have stronger responses to climate anomalies than those with longer generation
2392 time. *Nature communications* **12**, 1–8 (2021).

- [55] Le Coeur, C., Yoccoz, N. G., Salguero-Gómez, R. & Vindenes, Y. Life history adaptations to fluctuating environments: Combined effects of demographic buffering and lability. *Ecology Letters* **25**, 2107–2119 (2022). 2393
2394
2395
2396
2397
2398
2399
2400
2401
2402
2403
2404
2405
2406
2407
2408
2409
2410
2411
2412
2413
2414
2415
2416
2417
2418
2419
2420
2421
2422
2423
2424
2425
2426
2427
2428
2429
2430
2431
2432
2433
2434
2435
2436
2437
2438